Energy Advances

ROYAL SOCIETY OF CHEMISTRY

REVIEW ARTICLE

View Article Online
View Journal

Cite this: DOI: 10.1039/d6ya00028b

Transformative progress in anion-exchange membranes for fuel-cell technology

Parul Sharma and Anurag Prakash Sunda *

Anion-exchange-membrane fuel cells (AEMFCs) have gained significant attention in recent years due to their utilization of inexpensive metals. However, the conductivity of anion-exchange membranes in fuel cells still falls short when compared to the extensively researched proton-exchange-membrane fuel cells (PEMFC). Researchers at large are actively working towards the advancement of anion-exchange membranes that possess superior ionic conductivity, alkaline resistance, and mechanical stability. This work attempts to comprehensively review the recent transformative progress in attaining efficient anion-exchange membranes through both experimentation and computational approaches. The review delves into different aspects of anion-exchange-membrane performance, such as polymer structure, pendant group modifications, morphological traits, water management, *etc.*, to ensure high ionic conductivity and alkaline stability. Additionally, the review explores diverse strategies to protect the cationic functional groups to address the concern of deterioration. To understand the role of pivotal factors, insights are provided into the design of anion-exchange membranes with emphasis on high conductivity, enriched by summarizing recent advancements, including molecular studies. The alkaline stability and hydration control of anion-exchange membranes are key parameters to focus on for exceptional performance potential in forthcoming applications.

Received 7th February 2026,
Accepted 8th March 2026

DOI: 10.1039/d6ya00028b

rsc.li/energy-advances

1 Introduction

One of the biggest challenges in today's world is to find a balance between energy production and environmental pollution. The use of fossil fuels for generating energy or electricity is one of the leading causes of increasing environmental pollution. Fossil fuels liberate huge amounts of greenhouse gases, which adversely affect the environment and human health. Therefore, the use of renewable sources for the generation of energy or electricity has grown tremendously over the years, with improvement in the efficiency of solar cells, fuel cells, and super-capacitors. The best alternative to fossil fuels for generating energy is fuel cells.[1–3] Fuel cells convert chemical energy into electrical energy with minimal emission of pollutants.[4] Fuel cells generate zero noise pollution and possess high efficiency.[5,6] There are several types of fuel cells that operate under different conditions and use different types of materials, for example the proton-exchange-membrane fuel cell (PEMFC),[7,8] alkaline fuel cell (AFC),[9] anion-exchange-membrane fuel cell (AEMFC),[10] direct alcohol fuel cell (DAFC),[11] molten carbonate fuel cell (MCFC),[12] solid oxide fuel cell (SOFC),[13] and phosphoric acid fuel cell (PAFC).[14] All fuel cells consist of a cathode, anode, electrolyte, and fuel. At the anode, fuel is oxidized and releases electrons. At the cathode, air (oxidant) reacts with electrons and produces reduced species. Different fuel cells utilize different types of electrolytes and fuels.[15–18]

Among polymer-electrolyte-based fuel cells, the use of ion-exchange membranes as electrolytes in fuel cells has attracted tremendous attention. Ion-exchange membranes as electrolytes in fuel cells possess several advantages, such as they can operate at low temperatures, possess low corrosion risks, and are safe and easy to handle compared to liquid electrolytes. Ion-exchange membranes as electrolytes in fuel cells are classified as either proton-exchange membranes or AEMs, which result in the generation of either acidic or alkaline environments, respectively. Proton-exchange membranes allow protons to pass through selectively while preventing the passage of anions, whereas anion-exchange membranes perform the reverse action.[20] A schematic representation of various components of an AEM fuel cell is shown in Fig. 1. The comprehensive multiscale review by Lei and co-workers[21] primarily centred on electrochemical mechanisms in alkaline media, with particular emphasis on the hydrogen oxidation reaction (HOR), oxygen reduction reaction (ORR), catalyst design, and electrode-level processes. Its major strength lies in correlating reaction kinetics with electrocatalyst behavior across multiple scales.

The review of Yassin and Dekel[22] provided a broad, cross-cutting analysis of AEM-based technologies, including fuel

Department of Chemistry, J. C. Bose University of Science and Technology, YMCA, Faridabad – 121006, India. E-mail: anurag.sunda@gmail.com, anurag@jcboseust.ac.in

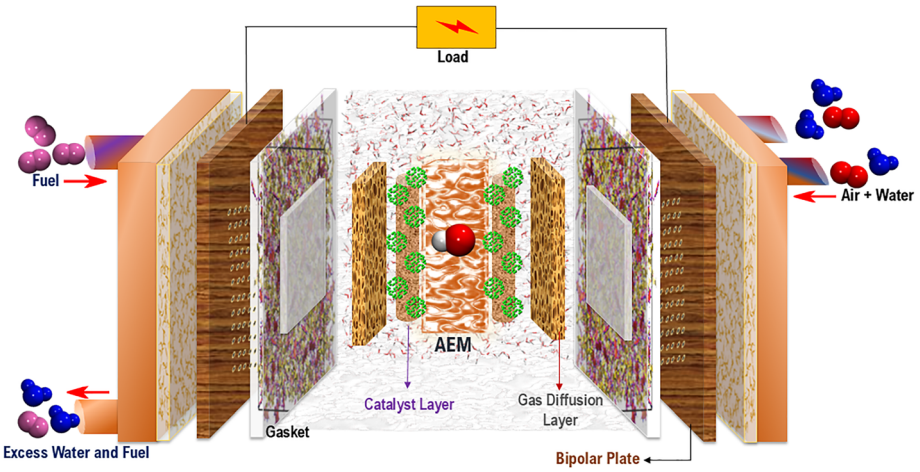

Fig. 1 A schematic representation of an AEMFC.

cells, water electrolyzers, redox flow batteries, CO_2 electrolysis systems, and gas separation platforms. While such wide-ranging scope was valuable for identifying common challenges across different electrochemical devices, it does not offer an in-depth, fuel-cell-specific membrane analysis. The recent review on membranes by Hsiao and co-workers[23] mainly focuses on comparative analyses of PEM and AEM water electrolyzers, alkaline-stability enhancement strategies, and patent-related developments.

In contrast to these prior works, our review is specifically centred on AEMs for fuel-cell applications, with a strong emphasis on membrane molecular design, polymer architecture engineering, and transport mechanisms. We provide a detailed mechanistic discussion of hydroxide ion transport, clarifying the interplay between vehicular and Grotthuss-type mechanisms under varying hydration conditions. Importantly, we include a separate and structured section dedicated to AEM synthesis methodologies, rational membrane design and

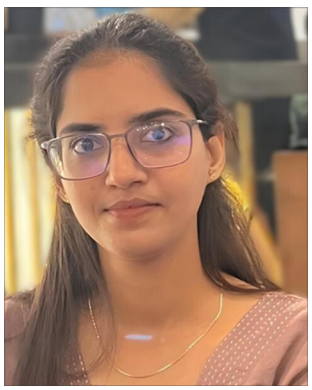

Parul Sharma

Parul obtained her master's degree in chemistry in 2021 from J. C. Bose University of Science and Technology, YMCA. In 2022, she joined the research group of Dr Sunda at the same institution to pursue her doctoral research. In recognition of her academic excellence and research potential, she was awarded the prestigious CSIR Junior Research Fellowship (JRF) in 2024 by the Council of Scientific and Industrial Research (India). Her research focus on fuel-cell technologies, with a specific focus on the molecular-level design and mechanistic understanding of anion-exchange membranes (AEMs). She employs advanced molecular dynamics simulations to elucidate their structural organization, ion transport behavior, and physicochemical properties, aiming to optimize membrane performance and durability for next-generation fuel-cell applications.

Anurag Prakash Sunda

Dr Anurag is an Assistant Professor of Chemistry at J. C. Bose University of Science and Technology, YMCA, serving since 2020. He earned his MSc (2008) and MPhil in Energy (2009) from the University of Rajasthan. He worked at the National Chemical Laboratory, Pune on polymer membranes before completing his PhD (2010–2014) at the Indian Institute of Science Education and Research (IISER, Pune). He subsequently pursued post-doctoral research at the JNCASR, Bangaluru. Dr Sunda received the prestigious DST INSPIRE Faculty Award in Materials Sciences (2015) from the Department of Science and Technology (DST), India and successfully completed the five year tenure (2015–2020). He was also awarded the Rajat Jayanti Science Communication Fellowship (2011) by the National Council for Science and Technology Communication. He has secured competitive grants including UGC Start-up (BSR) (2021), SERB/ANRF-CRG (2022), and HSCSIT DST-Haryana (2024). His research focuses on proton-conducting materials, electrolytes, ionic liquids, and polymer membranes for energy and environmental applications, with expertise in theoretical and materials chemistry.

fabrication. Furthermore, we present a systematic evaluation of recent strategies to enhance AEM performance, highlighting multiple emerging and innovative directions reported in the literature. A distinctive strength of our review is the dedicated integration of computational modelling approaches alongside experimental advancements, thereby bridging theory-guided design with practical material development. This review mainly puts emphasis on AEMs for alkaline anion-exchange-membrane fuel cells. The present work discusses the essential design aspects of anion-exchange membranes (AEMs) in relation to applications, specifically tailoring them to meet the demands of future energy in terms of stability, performance and durability.

2 Anion-exchange-membrane fuel cells

NASA used an alkaline fuel cell in the Apollo series missions and on the space shuttle. The world's first fuel-cell ship, 'The Hydra', used an alkaline fuel-cell system.[24] In these alkaline fuel-cell systems, liquid KOH electrolyte was used, which corrodes the electrode by forming K_2CO_3 on reaction with CO_2 present in the air.[10] To address this challenge, researchers opted for an anion-exchange membrane in place of a liquid electrolyte. In an AEM, the carbonate content is very low compared to a liquid electrolyte; hence, corrosion of the electrode does not occur. An AEMFC consists of a membrane electrode assembly (MEA) where the polymer electrolyte AEM connects a cathode and an anode *via* an active catalyst layer. Oxidation of hydrogen gas occurs at the anode and reduction of oxygen gas occurs at the cathode. The following reaction occurs at the cathode and anode in the fuel cell for electricity generation.[19]

$$\text{At the anode: } H_2 + 2OH^- \rightarrow 2H_2O + 2e^-$$

$$\text{At the cathode: } 1/2O_2 + H_2O + 2e^- \rightarrow 2OH^-$$

$$\text{Overall cell reaction: } H_2 + 1/2O_2 \rightarrow H_2O$$

AEMFCs have numerous advantages over PEMFCs, as summarized in Table 1. An AEMFC operates in an alkaline medium; therefore, the oxygen reduction reaction happens more effectively and easily compared to in a PEMFC.[25] In a PEMFC, highly expensive metal catalyst electrodes (*e.g.*, platinum) are used, which limits their usage at the industrial level, whereas an AEMFC can work with a low-cost non-platinum metal catalyst electrode (*e.g.*, silver, transition metal oxides). In the past few years, alkaline AEMFCs have gained popularity and become a hot research topic[26,27] because an increase in ionic conductivity up to 200 mS cm^{-1} has been recorded by several researchers.[28]

Table 1 Advantages and disadvantages of AEMFCs[9,10,19]

Advantages	Disadvantages
(1) Tolerance to CO poisoning	(1) Membrane degradation
(2) Non-precious metal catalysts	(2) Limited commercial availability
(3) Broader fuel flexibility	(3) Challenging to attain high hydroxide conductivity
(4) Environment friendly	(4) Limited operating temperature range

3 Anion-exchange membranes: role and performance

The AEM is a key component in an AEMFC because it is responsible for the transportation of hydroxide ions from the cathode to the anode.[29] An anion-exchange membrane is made up of a hydrophobic polymer backbone attached to a hydrophilic cationic head, in which the cationic head is responsible for the transportation of hydroxide ions from the cathode to the anode.[30] We can use poly(arylene ether), poly(2,6-dimethyl-1,4-phenylene oxide), poly(vinyl alcohol), poly(tetrafluoroethylene), *etc.* as the polymer backbone and quaternary ammonium, imidazolium and guanidinium ions, *etc.* as the cationic head groups for the AEM (see Table 2). Fumasep® FAA3, Tokuyama A201, Aemion™, Sustainion® 37–50, Durion TM1, and PiperION are some of the commercially available AEMs.[31,32] Commercially available AEMs face several limitations that impede their widespread adoption in various applications, for example limited alkaline stability, lower conductivity, water management (which presents another challenge as AEMs require careful hydration control), mechanical instability, *etc.* These obstacles have driven researchers to develop membranes capable of surpassing current constraints to enhance the performance of electrochemical devices such as fuel cells and water electrolysers.[33] Wang *et al.*[34] showed ion transport enhancement with the help of bromide ions, using poly(bromo butylnorbornene) homopolymer AEMs. The authors found that water percolation greatly relied on the local hydrated structure of the alkaline membrane. Du *et al.*[35] presented emerging concepts related to anion-exchange membranes as water electrolysers and highlighted the consideration of cross-linking or use of composites in AEMs to enhance alkaline stability.

3.1 Application of anion-exchange membranes in fuel cells

PEMFCs have been successfully adopted in fuel-cell electric vehicles, with commercial models introduced by Toyota Motor Corporation and Hyundai Motor Company, and General Motors confirming the practical viability of fuel cells in transportation. Despite these advancements, large-scale deployment of PEMFC technology remains restricted due to the reliance on costly platinum metal catalysts, durability concerns associated with acidic membranes, and the need for highly corrosion-resistant components.[3,49,50] In response to these limitations, AEMFCs have emerged as a promising alternative. Their operation in an alkaline medium allows the utilization of non-precious metal catalysts and more economically viable materials, thereby significantly reducing system cost.

Accordingly, AEMFCs are gaining considerable research interest as a viable alternative for next-generation energy conversion systems. To evaluate their practical feasibility and performance potential, extensive research efforts have focused

Table 2 Chemical structures of different polymer backbones and cationic heads groups

Polymer backbone units	Name of polymer	Ref.	Cationic head groups	Group name	Ref.
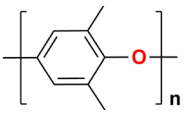	Polyphenyleneoxide	36	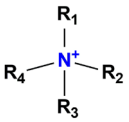	Quaternary ammonium	37
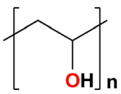	Polyvinylalcohol	38	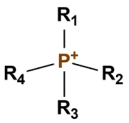	Phosphonium	39
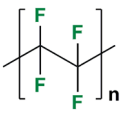	Polytetrafloroethylene	40	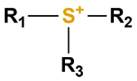	Sulfonium	41
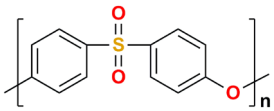	Polyethersulfone	42	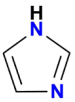	Imidazole	43
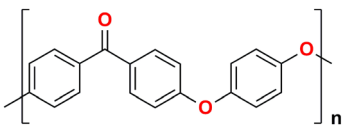	Polyetheretherketone	44		Pyrrolidine	45
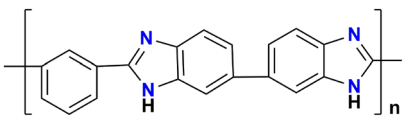	Polybenzimidazole	46	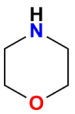	Morpholine	47
			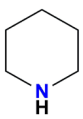	Piperidine	48

on the fabrication and single-cell testing of AEMFCs under optimized operating conditions. For instance, a series of polystyrene-*block*-polybutadiene-*block*-polystyrene (SBS) triblock copolymers functionalized with pyridinium groups (SBS-QA^+py) were synthesized and evaluated in alkaline single-cell fuel cells by Anley *et al.*[51] Within this series, SBS-$Qdpy_1$ and SBS-$Qdpy_2$ emerged as the most promising candidates due to their optimized balance between ion exchange capacity (IEC) and mechanical strength. Single-cell testing under fully humidified H_2/O_2 conditions (100% RH) at 80 °C and ambient pressure revealed peak power densities of 362.2 mW cm^{-2} for SBS-Qdpy1 and 398.1 mW cm^{-2} for SBS-$Qdpy_2$. These values exceeded the performance of the commercial Sustainion X37-50T (347 mW cm^{-2} under identical conditions) and were higher than that of PiperION-A20 (355–377 mW cm^{-2} under similar conditions with minor differences in backpressure).

A series of novel poly(fluorenyl aryl piperidinium) (PFAP) copolymers were designed by Chen and group[52] for both AEMs and anion-exchange ionomers (AEIs) to enhance AEMFC performance. The materials were systematically evaluated through single-cell H_2/O_2 fuel-cell testing under controlled temperature, humidity, and backpressure conditions to assess their practical applicability. Using PFBP-14 as the AEI and PFTP-13 as the AEM at 80 °C and 75%/100% RH, the cell delivered a peak power density of 1.67 W cm^{-2} without backpressure, which further increased to 2.34 W cm^{-1} under 1.3/1.3 bar backpressure. In contrast, commercial Fumatech-based AEMFCs typically achieve peak power densities of only 0.5 W cm^{-2}, highlighting the significant advancement offered by the PFAP-based system. In order to evaluate the effect of different amounts of hydrophobic fluorinated groups, PTF*x*-QAPTP AEMs were synthesized by Yu *et al.*[53] To assess their practical performance, single-cell fuel-cell tests were conducted. The PTF6-QAPTP membrane achieved a peak power density of 849 mW cm^{-2} at a current density of 1600 mA cm^{-2}, while PTF3-QAPTP delivered 571 mW cm^{-2}. The better performance of PTF6-QAPTP is likely due to its more distinct microphase separation, which leads to the formation of continuous and interconnected hydrophilic pathways.

3.2 Mechanism of hydroxide ion transport

Transportation of hydroxide ions occurs *via* AEMs involving different mechanisms, *e.g.*, the Grotthuss mechanism, surface site hopping, convection, and diffusion. An illustration of these mechanism around the AEM is presented in Fig. 2. In the Grotthuss mechanism, hydroxide ion transportation occurs by simultaneous breakage and formation of hydrogen bonds with water molecules. In surface site hopping, the surface site refers to the cationic group attached to the polymer backbone, and hydroxide ions hop from one cationic group to another present

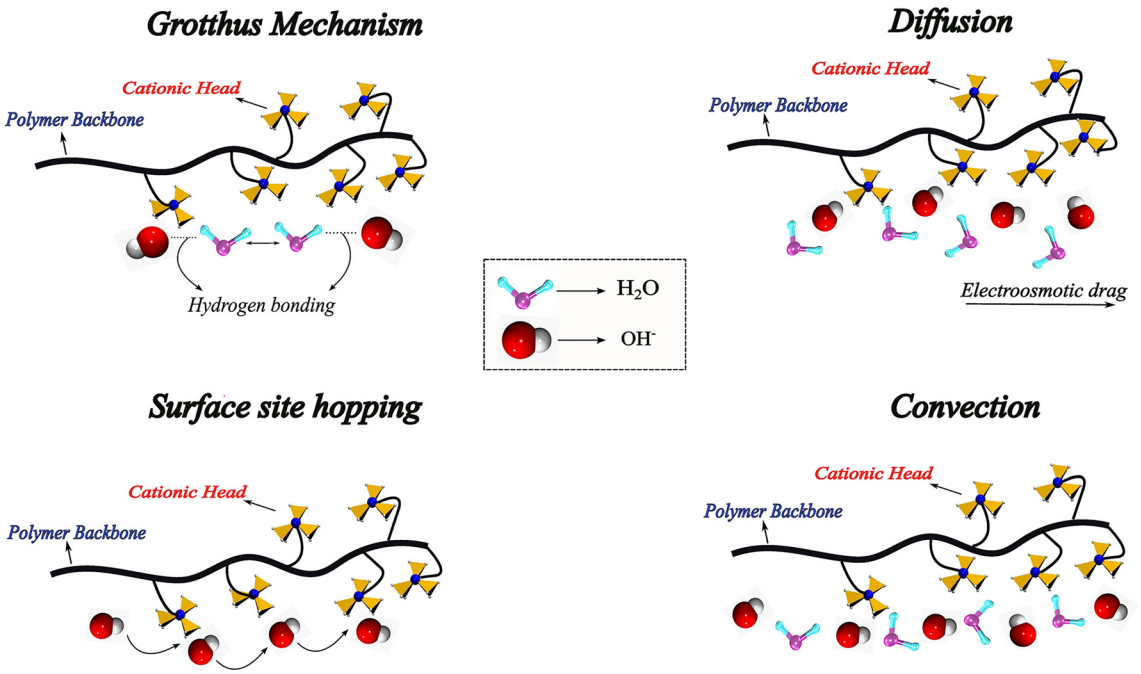

Fig. 2 A schematic representation of mechanisms involved in hydroxide ion transport.

in the anion-exchange membrane.[54] Diffusion occurs due to electroosmotic drag, where OH^- ions interact with water molecules and migrate across the membrane. The pressure gradient drives the convection transport of OH^- anions *via* the AEM membrane. As the OH^- ions move they carry water molecules with them through the membrane.[10,55] Enormous efforts have been made to get insights into ion transport in polymer electrolytes using different techniques. For example, Foglia *et al.*[56] used quasi-elastic neutron scattering to unveil characteristics of the ion dynamics in polymeric membranes, using the commercially available Fumatech FAD-55 membrane.

3.3 Performance of anion-exchange membranes

A good AEM should possess high hydroxide conductivity, and excellent thermal, chemical, and mechanical stability. In an anion-exchange membrane, the polymer backbone and the attached cation both contribute significantly to hydroxide conductivity and the stability of the membrane.[57] The performance of an AEM in an alkaline AEMFC depends on certain factors, such as ion exchange capacity, water uptake, alkaline stability, and the morphology of the membrane.[58] All these factors contribute significantly to hydroxide conductivity and membrane stability. In the last decade, a lot of research has been carried out on AEMs to attain hydroxide conductivity comparable to that of PEMFCs.

3.3.1 Ion exchange capacity. Ion exchange capacity (IEC) reflects the ability of the membrane to transport hydroxide ions. IEC indicates the number of functional groups available for ion exchange. A higher ion exchange capacity of the membrane leads to an increase in the hydroxide ion conductivity of the AEM. However, an excessive increase in the ion exchange capacity leads to swelling of the membrane, which results in overall disturbance of the morphology of the membrane.[59,60] The IEC is given as the number of mmol or mEq of exchangeable ions per gram weight of dry membrane.[61] Balancing the ion exchange capacity with other membrane properties, such as water uptake, and chemical and mechanical stability, is crucial in designing AEMs with better performance. The IEC is typically determined through three primary methods: potentiometric, titration, and spectrophotometric techniques. The potentiometric method involves measuring the change in pH resulting from an increase in OH^- concentration within the solution. The titration method is centered on titrating a membrane sample using $AgNO_3$ to determine the exchanged Cl^- and NO_3^- ions. Meanwhile, the spectrophotometric detection method relies on the identification of NO_3^- ions exchanged with Cl^- ions within the membrane sample.[62]

3.3.2 Membrane morphology. The morphology of polymer membranes holds significant importance; it acts as a pivotal stabilizing element and significantly influences hydroxide ion mobility. This micro-phase separation morphology observed in AEMs results from the distinct characteristics of their hydrophobic and hydrophilic segments. The formed morphology is greatly influenced by the properties of the cationic head group, the polymer backbone, and the manner in which these components are interconnected.[63] By gaining a well-defined morphology, it is possible to enhance the ion transport pathways within the membrane, facilitating faster and more efficient ion exchange. This, in turn, leads to improved overall electrochemical device performance. Additionally, it can help mitigate issues related to membrane swelling and stability, ensuring long-term durability and consistent operation. To examine the

microscopic structure of AEMs, researchers typically employ transmission electron microscopy (TEM), atomic force microscopy (AFM), and small-angle X-ray scattering (SAXS) as primary techniques.[64] Frischknecht and co-workers[65,66] employed molecular simulations with different cation heads on polysulfone- and poly(aryl piperidinium)-based AEMs. The authors explored hydroxide ion percolation through water domains in a membrane matrix. Barnett *et al.*[67] showed the role of hydrophilic channels in nanophase-segregated polyphenylene oxide (PPO)-based AEMs. Drayer *et al.*[68] explored the role of trimethylammonium and dimethyl-hexyl ammonium pendant groups attached to a polyethylene backbone. The morphological traits revealed widening of hydrophilic channels to enhance water percolation with an increase in hydration.

3.3.3 Water management. Water management also plays a vital role in AEM stability, as water is generated at the anode and it is needed at the cathode for the reduction of oxygen. A higher current density of the cell may lead to dryness of the cathode and may cause waterlogging at the anode. Moreover, excessive water uptake can result in membrane swelling, which can cause a breakdown in the mechanical and chemical characteristics of the membrane. Apart from hydration, the concentration of hydroxide ions is equally crucial for optimum performance. Razmjooei *et al.*[69] explored the cell performance at varying KOH concentration and obtained the highest cell performance at 1 M concentration of KOH. A further increase in hydroxide ion concentration limits cell performance due to membrane resistance. In order to achieve the best possible membrane performance, it is essential to maintain an optimum level of hydration.[70,71]

For water uptake measurements, the process involves several steps. First, the membrane samples are converted to the hydroxide form. Following that, they are dried until a consistent mass is achieved and then weighed, while the length of the membrane is measured. Next, these dried membrane samples are placed in a sealed container filled with water, typically for a period of 24 hours. After the immersion period, any excess surface water on the membranes is quickly removed by wiping with tissue paper. Immediately after this, the membranes are weighed and their dimensions are measured. The collected data from these steps are then used to calculate two important parameters: water uptake (WU) and swelling ratio (SR). In essence, this process assesses how much water the membrane can absorb and how much it swells when submerged, providing valuable information about its water-handling characteristics.[10] Zheng *et al.*[72] investigated fluorinated and hydrocarbon-based AEMs to explore role of water uptake and its kinetics. The authors found a characteristic time for water uptake for AEMs that varies with the polymer backbone, membrane structure, temperature and humidity level. Xu *et al.*[73] demonstrated the importance of anisotropic swelling with hydration of the AEM, which facilitates ion transport effectively by filling the gap between the interface of the catalyst layer and the membrane.

3.3.4 Alkaline stability. Highly reactive OH^- ions degrade the cationic head attached to the polymer membrane at temperatures above 60 °C *via* several mechanisms, *e.g.*, Hoffman elimination, nucleophilic substitution reaction, and formation of reversible ylides through the attack of hydroxide ions at the alpha-hydrogen position.[74–76] It is also found that nitrogen-based cationic groups are more chemically stable compared to phosphonium or sulfonium.[77] Li *et al.*[78] presented the role of a quaternized polystyrene-based electrode binder at very high pH to address the alkaline stability of the electrolysers. Heterocyclic anion-exchange groups, such as imidazolium or pyridinium, demonstrate superior stability due to their conjugated structure and steric hindrance.[79] The degradation is not limited solely to the cationic head; instead, the polymer backbone, which includes electron-withdrawing groups like ether bonds, also tends to deteriorate when exposed to an attack. Su *et al.*[80] prepared a novel aryl-ether-free piperidinium-functionalized SEBS (SEBS-Pi) alkaline membrane. The SEBS-Pi membrane demonstrates excellent resistance to alkaline conditions, as it remains stable for 576 hours at 80 °C in a 1 M KOH solution. Furthermore, it retains high levels of ion exchange capacity and conductivity, and there are no apparent alterations in its FT-IR spectra, indicating its robust resistance to an alkaline environment. Min *et al.*[81] reported an approach to designing a stable AEM in an alkaline environment by crosslinking two different aryl-ether-free polymers, poly(m-terphenyl *N*-methyl piperidine) (PmTP) and poly(styrene-*b*-ethylene-*co*-butylene-*b*-styrene) (SEBS). The membrane displayed exceptional alkaline stability by retaining approximately 99% of its initial conductivity and IEC, even after being immersed in a 2 M KOH solution at 80 °C for a duration of 600 hours. Yuan and team[82] introduced an innovative method to create a stable AEM by employing an organometallic cationic head. They utilized poly(isatin biphenylene) as the hydrophobic polymer backbone and $[Cp–Fe–toluene]^+$ as the hydrophilic cationic head. Remarkably, the resulting membrane exhibited exceptional durability, lasting for 1000 hours in 1 M KOH at 60 °C, while retaining 81.4% of its hydroxide conductivity.

The Dekel and Diesendruck group have put immense efforts into systemically examining the alkaline stability of AEMs, specifically targeting quaternary ammonium cation heads with various polymer backbones.[83–87] The kinetic stability of quaternary ammonium cations is greatly influenced by membrane hydration and low hydration is less favourable for prolonged stability of the membrane. The authors suggested that the isoindolinium group can be a very good alternative for replacement of quaternary ammonium cation heads at low hydration or under dried conditions.[88]

A well-planned molecular design to enhance the alkaline durability of AEMs was introduced by Wang and team.[89] Rather than altering the polymer backbone or introducing a new cationic headgroup, the authors showed that a simple positional isomerization of the piperidinium linkage can significantly improve membrane durability. Notably, both conventional PAP and the isomeric i-PAP share the same ether-free arylene backbone and identical piperidinium cations; the only structural difference lies in the attachment position of the nitrogen atom. This subtle yet important modification alters the local molecular

geometry around the cationic center. As a result, the dominant Hofmann elimination pathway is significantly suppressed, leading to enhanced alkaline stability without compromising the original backbone or polymer structure. After immersion in 10 M aqueous NaOH at 80 °C for 360 h, the decomposition of piperidinium groups in the isomeric i-PAP membrane was approximately half of that observed in the conventional PAP membrane.

Another approach by Liu and coworkers[90] reported the development of poly(diphenyl carbazole)-based AEMs incorporating multi-cationic alkoxy side chains. By precisely tuning the alkoxy chain in terms of carbazole content, the authors reported ordered ion transport channels through multi-cation dipole interactions, achieving high hydroxide conductivity of 154.6 mS cm^{-1} at 80 °C. Importantly, the introduction of an alkoxy chain (QPDPC-O-20) rather than only an alkyl chain (QPDPC-C-20) enhanced alkaline stability by promoting stronger intermolecular interactions and better water regulation, leading to 98.3% conductivity retention after 2000 h in 1 M KOH. However, after 600 hours in an alkaline solution of 5 M KOH, the QPDPC-O-20 membrane was able to maintain about 71.4% of its original conductivity, while the QPDPC-C-20 membrane retained 63.2%, indicating better stability of the alkoxy-modified membrane.

Wang *et al.*[91] investigated poly(biphenylene alkylene)-based AEMs, PBPA*n*QA (n = 4, 5, 6), where n represents the alkylene spacer length between the backbone and the quaternary ammonium groups. The main objective was to systematically investigate how spacer length influences alkaline stability. The membranes were immersed in 5 M NaOH at 80 °C for 1000 h. Changes in chloride conductivity at 80 °C and structural variations from ^{1}H NMR spectra were analyzed before and after alkaline treatment. After 1000 h aging, PBPA6QA (with a hexylene spacer) showed a conductivity decrease of only 21%, from 42.5 to 33.4 mS cm^{-1}. In contrast, PBPA5QA and PBPA4QA exhibited higher conductivity losses of 35% and 46%, respectively. This trend was consistent with the extent of QA cation degradation: 18.3% for PBPA6QA, 22.7% for PBPA5QA, and 35.2% for PBPA4QA. The results clearly demonstrate that increasing the alkylene spacer length enhances alkaline stability.

3.3.5 Mechanical stability. Mechanical stability of AEM mainly depends on the polymer backbone. Mechanical degradation happens mainly because of the physical and chemical stress present in the fuel cell. An optimal amount of IEC, and appropriate WU and SR are necessary to maintain the mechanical strength of an AEM. The ASTM D-1708 method is used to evaluate the mechanical properties of AEMs, including tensile strength, modulus of elasticity, and elongation at break. Crosslinking of membranes helps in increasing the mechanical strength of AEMs.[10,92] The crosslinked membrane designed by Min *et al.*[81] exhibited Young's modulus of 486 MPa and a high elongation at break of 70.3% at a crosslinking degree of 40%. Chen and their research team[93] created an alternative crosslinked membrane by combining di-piperidinium and poly(fluorenyl-*co*-terphenyl piperidinium), allowing for a customizable alkyl spacer. This engineered membrane exhibited favorable mechanical characteristics, including a tensile strength of around 90 MPa and an elongation at break of approximately 35%. To tackle the balance between the conductivity and stability of AEMs, Guo *et al.*[94] designed an AEM using a PBI copolymer containing norbornene, the crosslinked network being obtained *via* the 'thiol–ene' click chemical reaction during membrane fabrication. The fabricated membrane exhibited a tensile strength of 47.75 MPa, elongation at break of 31.89% and SR of less than 15%. Das and team[95] developed a series of ionically cross-linked AEMs by blending pyridine-bridged polybenzimidazole (PyPBI) and N-spirocyclic quaternary ammonium spiro ionene polymer (SP). The membrane showed a maximum tensile strength of 35.23 MPa and elongation at break of 37.14%.

Researchers have been actively conducting extensive studies at both experimental and theoretical levels to preserve specific properties and develop a suitable AEM. Substituted imidazolium groups generally exhibit higher alkaline stability than unsubstituted imidazolium due to reduced proton abstraction and improved steric protection. In piperidinium-based AEMs, *N*-methyl substitution at the 3-position results in superior alkaline stability compared to substitution at the 4-position, as reported in the work of Peng *et al.*[96] These efforts aim to enhance hydroxide conductivity while ensuring the membrane's chemical and mechanical stability, along with balancing the IEC and water uptake. Motealleh and co-workers[97] evaluated the durability of an imidazolium-functionalized AEM based on styrene (Sustainion) polymer and found a stable performance of 1 A cm^{-2} at 1.85 V for potential commercial application.

4 Synthesis methods of anion-exchange membranes

4.1 Solution-casting method

The most promising conventional method for production of AEMs is the solution-casting method (see Fig. 3). This process has four steps: dissolving the polymer, adding a functional group by chloromethylation, quaternizing it and casting it as a film. This method applies to soluble polymers, copolymers and their blends. The procedure involves dissolving the chosen polymer in a compatible solvent to form a uniform solution. Then the cation functional group is introduced *via* chloromethylation. This solution is subsequently spread or cast evenly onto an appropriate surface. As the solvent gradually evaporates, the polymer material solidifies, leading to the formation of a thin membrane.[98] Samsudin *et al.*[99] designed a composite AEM applying the solution-casting method using poly(vinyl alcohol) (PVA), poly(diallyldimethylammonium chloride) (PDDA), and nanozirconia (NZ). The designed membrane showed OH^- conductivity of 31.6 mS cm^{-1} at ambient temperature. The incorporation of NZ results in a low water uptake and swelling ratio. Wang *et al.*[100] used the solution-casting method in their synthesis process for membranes. The authors used a triple block copolymer, poly(styrene-*b*-(ethylene-*co*-butylene)-*b*-styrene), and quaternary ammonium functional groups. The designed membrane showed

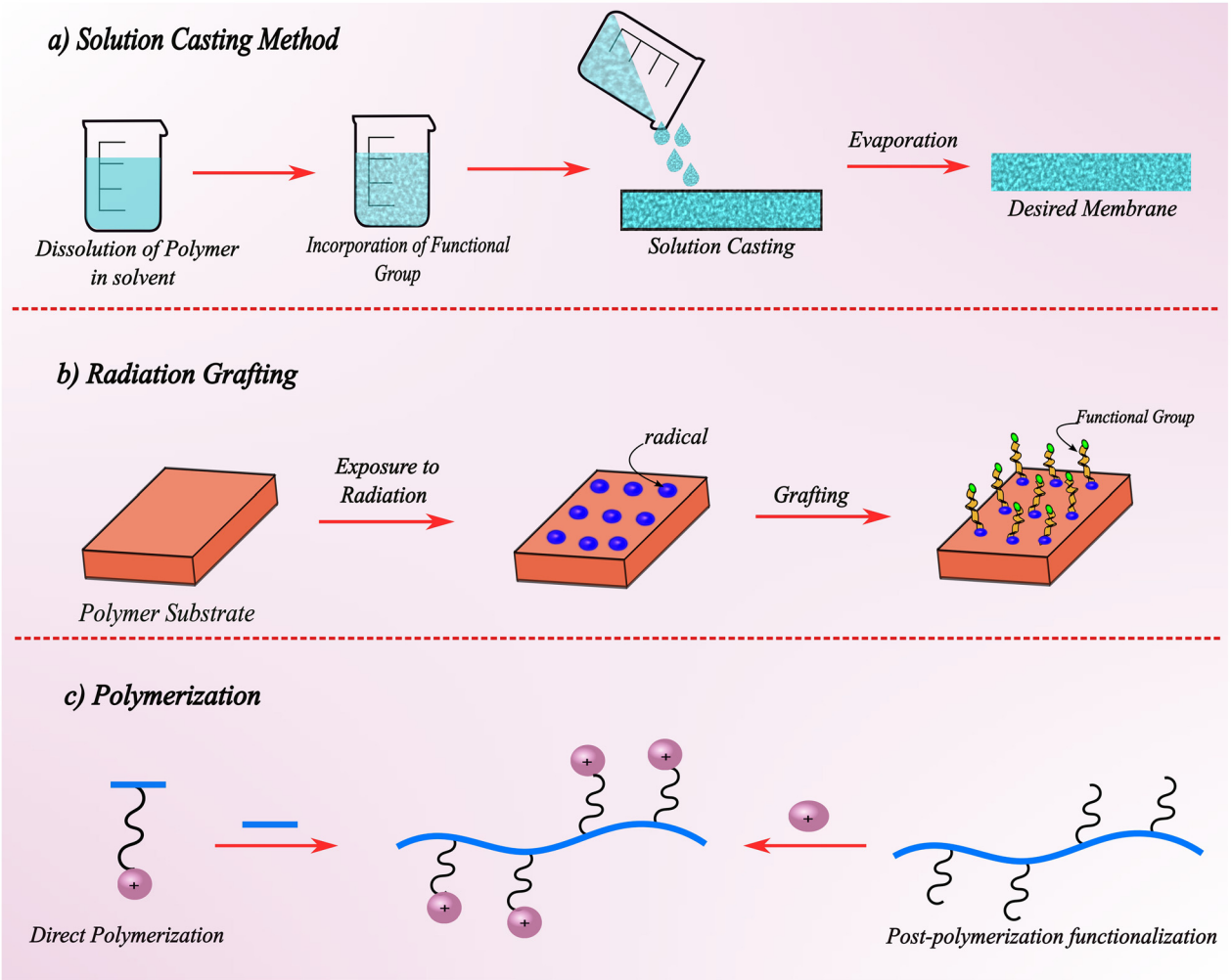

Fig. 3 A schematic representation of different synthesis methods of AEMs.

an OH^- conductivity of 72.13 mS cm^{-1}, swelling ratio of 9.3% and current density of 350 mA cm^{-1} at 80 °C.

4.2 Radiation grafting

Radiation grafting involves grafting of the functional groups onto the polymer membrane using radiation such as gamma rays or electron beams. This process starts with a pre-existing polymer substrate. The polymer substrate is then exposed to ionizing radiation, which generates radicals within the polymer matrix. The generated radicals initiate a grafting reaction between the polymer matrix and the selected monomer functional groups, leading to the integration of functional groups.[3,98] Wang *et al.*[101] reported hydroxide ion conductivity of 200 mS cm^{-1} at 80 °C using a 30 μm thick LDPE (low-density polyethylene)-based radiation-grafted anion-exchange membrane (RG-AEM). Biancolli *et al.*[102] designed a radiation-grafted ETFE-based AEM and analysed the effect of irradiation conditions on the membrane. It was observed that subjecting the membrane to ionizing radiation doses below 40 kGy, while maintaining an inert N_2 atmosphere apart from air, resulted in improved stability for the polymer backbone and enhanced alkaline resistance of the membrane. Biancolli and coworkers[103] illustrated the use of radiation and tailored thickness of the polymer film to improve the ion-exchange capacity of AEMs.

4.3 Polymerization

Polymerization processes are divided into two main categories: direct polymerization (DP) and post-polymerization functionalization (PPF). In direct polymerization, cationic monomers are created and then subjected to the polymerization process. Conversely, in PPF, cationic functional groups are introduced onto pre-formed polymer backbones.[104] There are several types of DP methods, which include ring-opening-metathesis polymerization (ROMP) and radical polymerization. The ROMP method[105] is used to polymerize cyclic alkenes. It involves the opening of the ring structure to form linear polymer chains, catalyzed by Ru complexes known as Grubbs' catalysts.[106,107] Radical polymerization involves generation of radicals to initiate polymerization reactions. Peroxides or azo compounds are used to generate free radicals. Singh and coworkers[108] developed an innovative di-quaternized cross-linked AEM using 1,4-bis(4-vinylbenzyl)-1,4-diazabicyclo[2,2,2]octane-1,4-diium (BVDOD) as a cross-linking agent and poly(vinylidene fluoride-*co*-hexafluoro

propylene) (DHPVDF-*co*-HFP) as the polymer backbone through the radical polymerization method. Azobisisobutyronitrile (AIBN) was employed by the researchers as an initiator for free radicals. The newly created cross-linked AEM demonstrated an ion exchange capacity of 1.02×10^{-3} equivalents per gram and a hydroxide ion conductivity of 57 mS cm^{-1} at a temperature of 30 °C. All the membrane preparation methods are illustrated through pictorial representations in Fig. 3.

5 Recent progress in anion-exchange membranes

Researchers have implemented various strategies to address issues such as the deterioration of the cationic head and the instability of the polymer's backbone. They have focused on enhancing the conductivity of hydroxide ions and achieving a well-defined morphology. These efforts have involved the creation of polymers with distinct structures, including block, comb-shaped, graft, and cross-linked polymers that incorporate cations (see Fig. 4). These structural modifications have led to the formation of micro-phase separation structures, resulting in improved conductivity, reduced swelling effects, and enhanced stability in an alkaline environment. The key performance-enhancement strategies can be identified as follows:

- Molecular structure engineering of cationic groups
- Polymer backbone optimization
- Crosslinking and network design
- Hydrogen-bonding network construction
- Branched and hyperbranched polymer architectures
- Grafting and side-chain engineering approaches

These strategies place emphasis on controlled phase separation, ion-channel formation, mechanical reinforcement, and multiple hydrogen-bonding networks to improve dimensional stability, water retention, and ion transport efficiency. The emerging design dimensions in AEM development demonstrate performance competitiveness with proton-exchange membranes,[109] supporting a rational approach to membrane engineering.

Recent research has focused on creating multiple hydrogen-bonding sites within the polymer structure to facilitate efficient OH ion transport and enhance the overall performance of the AEM. In this context, Wang and group[110] developed an AEM based on a poly(oxindole benzofuran) backbone incorporating quaternary ammonium functional groups for efficient OH ion transport. In addition to the oxindole moieties, hydroxyl (–OH) groups were introduced into the side chains to promote multiple hydrogen-bonding interactions. The P(O-$F_{50\%}$-$C_{50\%}$)-GTA membrane demonstrated a high hydroxide ionic conductivity of 103 mS cm^{-1} at 80 °C. The membrane maintained acceptable mechanical strength (8.6 MPa). The *ex situ* alkaline stability tests revealed that the membrane retained more than 80% of its initial conductivity after 600 h.

Peng *et al.*[111] studied a poly(terphenyl)-based AEM functionalized with quaternary ammonium groups along with incorporation of heteroaromatic units (*e.g.*, thiophene/furan units). The results indicated that introduction of thiophene units into the polymer backbone significantly enhanced membrane performance with QP(TP_{30}-*co*-DBT_{70}) showing a hydroxide conductivity of 120 mS cm^{-1} at 80 °C, mechanical strength of 26.6 MPa, and a relatively low volume swelling ratio of 34.6%.

In the study conducted by Li and co-workers,[114] an AEM was developed using polyphenylene oxide (PPO) that featured a comb-like structure. The cationic heads consisted of quaternary ammonium and were linked to a lengthy alkyl chain. This substantially decreased the swelling ratio and decreased the probability of nucleophilic attack of hydroxide ions on the cationic head. Zhang *et al.*[115] developed a bent twisted block

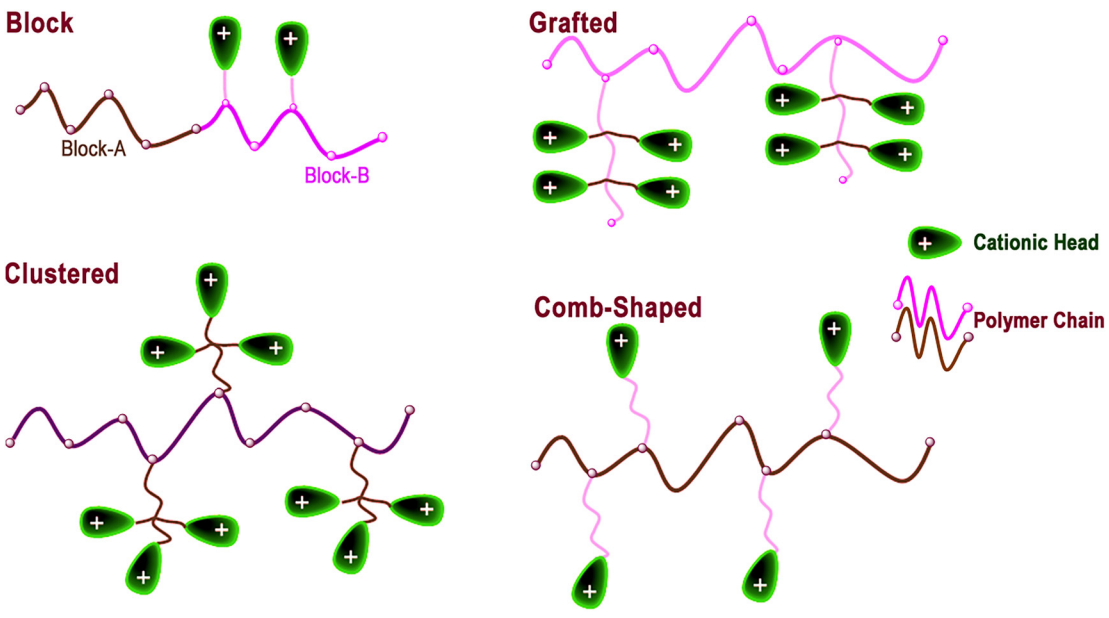

Fig. 4 A schematic representation of different types of polymers from AEMs (recreated from Xu, Su and Lin,[64] copyright 2020).

copolymer with 1,2-dimethyl imidazolium cations and attained a hydroxide conductivity of 35 mS cm^{-1} at room temperature. The fuel cell employed with this membrane showed a peak power density of 262 mW cm^{-2} at 50 °C. Chen *et al.*[116] created a graft polymer using perfluorinated poly(diphenylene) with the alkoxy side chain of a piperidinium quaternary ammonium salt. A well-defined microphase-separated structure was found that improved the ionic conductivity. Their group analyzed the membrane by taking different lengths of side chains and witnessed an ionic conductivity of 80 mS cm^{-1} at 80 °C; the swelling ratio was also low at approximately 17.1%, and the power density was about 1.008 W cm^{-2} for the long-side-chain polymer. Wang and team[117] crafted a branched poly(*p*-terphenyl triphenylmethane 1-methyl piperidine) anion-exchange membrane and reported a high hydroxide conductivity and alkaline stability. To boost conductivity, the branched membrane was crosslinked using multiple cations. The cross-linked version showed a tremendous increase in hydroxide conductivity of about 155.3 mS cm^{-1} at 80 °C. Wu *et al.*[118] created an anion-exchange membrane composed of branched poly(aryl piperidinium). The synthesized membrane showed minimal water absorption and swelling. The research team discovered that this branched membrane displayed outstanding resistance to alkaline conditions and demonstrated a commendable hydroxide conductivity of approximately 145 mS cm^{-1} at 80 °C. Lee *et al.*[119] produced an anion-exchange membrane utilizing Nafion and Aquivion-based perfluorinated precursors with trimethyl ammonium (TMA) cations. The authors conducted a comparison of properties like conductivity, morphology, and alkaline stability between Nafion and Aquivion-based AEMs and a commercial hydrocarbon-based Fumatech ionomer. The results indicated that all three membranes exhibited a phase-separated structure. The perfluorinated membrane displayed more pronounced phase separation due to its exceptionally high hydrophobic characteristics. Furthermore, the impact of relative humidity on membrane conductivity showed that perfluorinated membranes consistently exhibited superior conductivity at all humidity levels when compared with commercial Fumatech membranes. Lai *et al.*[112] synthesized an AEM using block polymer poly(arylene ether nitrile ketone) (QFPENK-*m*-*n*) as a main chain, combining it with comb-shaped alkyl side chains. The morphology of QFPENK-*m*-*n* with varying *m* and *n* values is shown in the Fig. 5a–f. The AEM showed a well-defined phase-separated microphase morphology and hydroxide conductivity up to 34.3 mS cm^{-1} at 30 °C and 102.1 mS cm^{-1} at 80 °C. It was also observed that an increase in the hydrophobic segment resulted in a reduction in both water uptake and the percentage SR (see Fig. 5g).

Huang *et al.*[113] designed an AEM using poly(*p*-terphenyl-*co*-1,2-diphenyl ethane piperidinium) (PDTP). To produce a high-performance AEM named 'PDTP-BMP-*x*C', their procedure included the crosslinking of the PDTP backbone, wherein the variable '*x*' denotes the extent of the crosslinker's length. It was observed that PDTP-BMP-6C exhibited a conductivity of 104.61 mS cm^{-1} when measured at 80 °C. Additionally, its power density at the same temperature reached 214 mW cm^{-2}. The micro-phase morphology structure for the crosslinked membrane PDTP-BMP-*x*C can be seen in the Fig. 6.

Chen *et al.*[121] designed a poly(crown ether) (PCE)-based AEM-QAPCE-*x*C, where *x* represents the length of the alkyl chain. A quaternary ammonium cationic side chain was employed, and the PCE backbone was crosslinked using various alkyl chain lengths. Reportedly, QAPCE-16C exhibited an impressive ionic conductivity of 125 mS cm^{-1} at 80 °C. Furthermore, QAPCE-16C demonstrated favorable dimensional stability, as well as robust mechanical and thermal durability. Mandal *et al.*[122] investigated the role of homopolymer, random and block polymerization in poly(norbornene) AEMs. The authors found that block-polymer performance had an edge over the random polymer structure, with a power density of 3.21 W cm^{-2}. Caielli and team[123] achieved a remarkable result in hydroxide conductivity, reaching 185 mS cm^{-1} at a temperature of 80 °C. This was accomplished through the creation of a membrane utilizing poly(aryl piperidinium) (PAP). Tao Wang and coworkers[124] documented an extraordinarily elevated

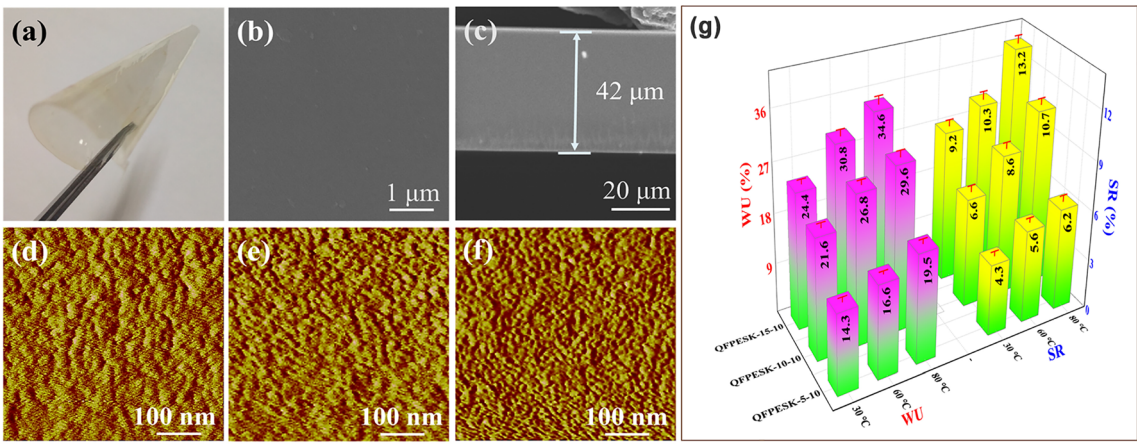

Fig. 5 (a) Digital photo of the membrane, and (b) membrane cross-section and (c) surface SEM images of QFPESK-10-10; AFM phase images of (d)–(f) QFPESK-5-10, QFPESK-10-10 and QFPESK-15-10, respectively; (g) water uptake and swelling ratio of the QFPENK-*m*-*n* AEMs at different temperatures. This figure has been adapted/reproduced from Lai *et al.*[112] with permission from John Wiley & Sons, Inc., copyright 2024.

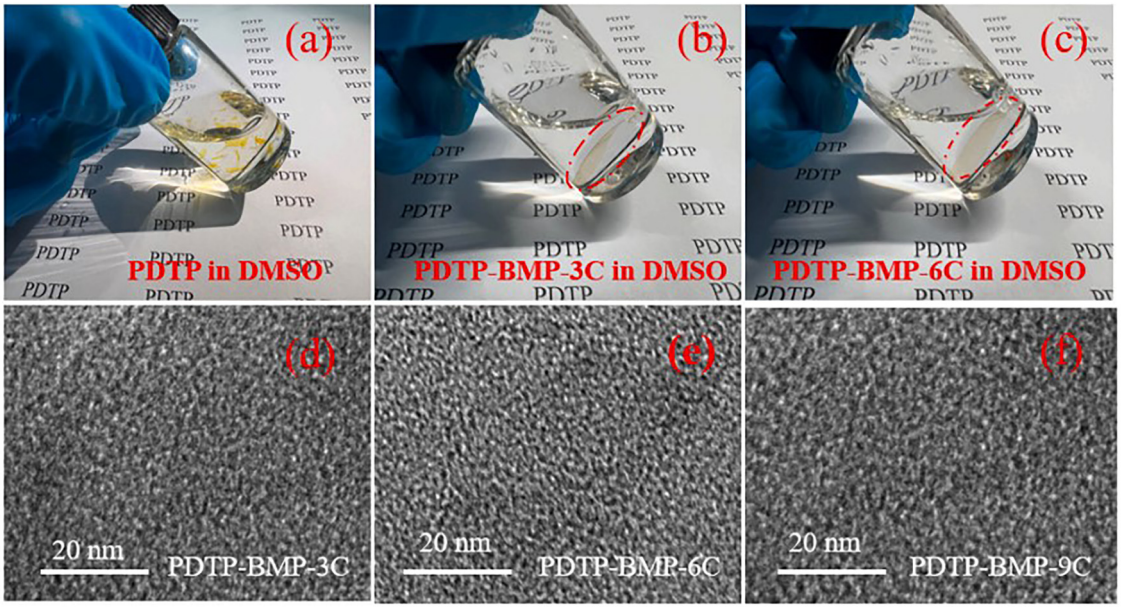

Fig. 6 (a)–(c) Digital photos of the PDTP, PDTP-BMP-3C and PDTP-BMP-6C membranes immersed in DMSO; (d)–(f) TEM images of the membranes. This figure has been adapted/reproduced from Huang *et al.*[113] with permission from Elsevier, copyright 2023.

hydroxide conductivity of 227.8 mS cm^{-1} at 80 °C, employing an AEM based on poly(arylene alkylene). Their research group created a membrane composed of a poly(*q*-tetraphenylene-*co*-*p*-terphenylene alkylene) rigid backbone, integrating the quaternary ammonium cationic functional group. Wu and co-workers[125] pursued a method for creating a notably effective AEM by applying a fluorination technique to the structure of poly(aryl piperidinium) (PAP). As a result, the fluorinated anion-exchange membrane (FPAP) displayed exceptional dimensional stability with a SR below 20 percent. The membrane exhibited remarkable mechanical characteristics, and the researchers observed tremendously high conductivity exceeding 150 mS cm^{-1} at 80 °C.

Zhang and their research team[126] utilized covalent organic frameworks (COFs) to create an AEM. They synthesized a composite AEM by combining COF-$DhaTG_{Cl}$ with PPO. Initially, they prepared a few-layered nanosheet structure using COF-$DhaTG_{Cl}$, and then introduced quaternary ammonium-functionalized PPO into these nanosheets. Their findings showed that at a doping level of 20 wt%, the conductivity of OH^- ions reached 148.65 mS cm^{-1} at 80 °C, while at a doping level of 30%, the conductivity was measured at 136.52 mS cm^{-1} at the same temperature. The reason for this decrease in conductivity can be attributed to the aggregation of COF-$DhaTG_{Cl}$ nanosheets within the membrane, which hinders the internal conduction pathways. Ju *et al.*[127] conducted synthesis of an AEM based on poly(arylene ether ketone). They achieved this by employing Friedel–Crafts acylation, followed by the introduction of imidazole cationic groups through a bromination reaction. Their work yielded impressive results, with the AEM displaying its highest hydroxide conductivity of 126.6 mS cm^{-1} at an operating temperature of 80 °C. Additionally, they observed a peak power density of 389.71 mW cm^{-2}. A partially fluorinated membrane (PFBE-*co*-VBC) with quaternary ammonium functional groups was successfully created by Hosimin and co-workers.[120] The researchers also created a blended AEM by combining PFBE-*co*-VBC with PVDF. Analysis using FE-SEM revealed an interconnected network structure in the AEM (see Fig. 7). The blended membrane, with a 1 : 1 ratio, demonstrated an ion conductivity of 1.0×10^{-2} S cm^{-1} and an ion-exchange capacity of 1.7 mmol g^{-1}.

Arunkumar and team[128] devised a method to enhance the properties of the commercially available FAA3 AEM. They achieved this by incorporating carboxylic-acid-functionalized graphene nanofibers into the FAA3 matrix. Introducing these graphene nanofibers significantly improved the electrochemical performance and chemical stability of the FAA3 membrane. The original FAA3 membrane had a hydroxide conductivity of 28.7 mS cm^{-1}, whereas the nanocomposite membrane with 1.70 wt% of nanofibers showed an enhanced conductivity of 58.8 mS cm^{-1} at 90 °C. Lee *et al.*[129] created various PPO-based AEMs with quaternary ammonium groups having different side-chain lengths. Their observations revealed that when the lengths were similar, the crosslinked membranes demonstrated superior alkaline stability in comparison to their non-crosslinked counterparts. Specifically, the crosslinked cQPH membrane with a hexyl acyl chain exhibited an anion conductivity of 105 mS cm^{-1} at 80 °C due to effective phase separation. The various attempts in the recent development of novel AEMs and their performance are provided in Table 3.

Hu *et al.*[130] focused on backbone structure modification by introducing alkyl spacers of varying lengths (n = 0, 1, 2, 6, and 10) into poly(aryl-*co*-terphenyl piperidinium) (PD_nTP-x) polymers. Short spacer membranes (n = 0–2) exhibited efficient ionic aggregation and continuous hydroxide transport pathways, achieving conductivities exceeding 150 mS cm^{-1} at 80 °C.

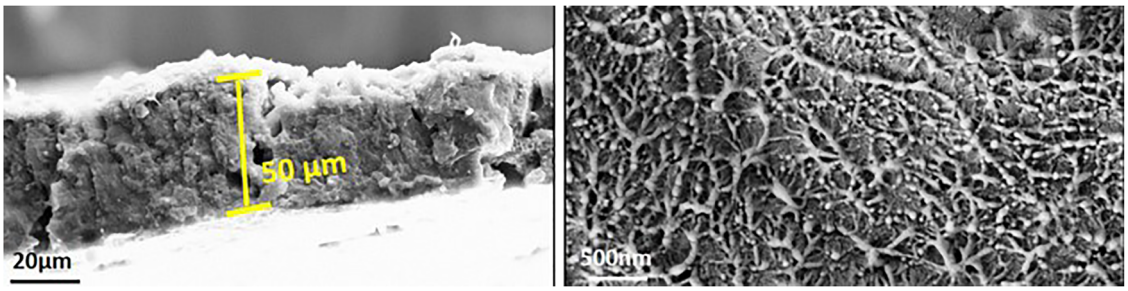

Fig. 7 FE-SEM cross-sectional images of a blended anion-exchange membrane (1 : 0.33). This figure has been adapted/reproduced from Hosimin *et al.*[120] with permission from the Royal Society of Chemistry, copyright 2023.

Notably, the PD_0TP-*x* membrane delivered a record peak power density of 2.67 W cm^{-2}. Conversely, Kim *et al.*[131] employed a side-chain modification strategy, keeping the same polymer backbone and cationic head as in the work of Hu and group, in which a hexyl alkyl chain spacer was introduced between the rigid polymer backbone and the cationic head group. This architecture promoted distinct microphase separation and optimized water management, leading to hydroxide conductivities exceeding 120 mS cm^{-1} and peak power densities up to 1.47 W cm^{-2}. Overall, these studies demonstrate that precise molecular-level modification, either through backbone or side-chain modifications, critically enhances ion transport, stability, and fuel-cell performance, underscoring the strong structure-modification–performance relationship in AEM design.

6 Computational approach to anion-exchange membranes

Computational techniques provide a deep understanding of molecular interactions, enabling researchers to adapt properties for specific applications. Through simulations, researchers can predict the performance of membranes before their actual synthesis. The requirement for extensive experimental trials is considerably reduced by computational simulations, resulting in faster and more affordable membrane design.[147,148] Gu *et al.*[149] analysed different N3-substituted imidazolium-based AEMs, with 1,2-dimethyl-3-isopropylimidazolium $[DMIIm]^+$, 1,2-dimethyl-3-butyl imidazolium $[DMBIm]^+$, and 1,2,3-trimethyl-imidazolium $[TMIm]^+$ ions, in aqueous solution through density functional theory. They reported that $[TMIm]^+$ exhibited the lowest LUMO energy; hence, the probability of getting degraded by the nucleophilic attack of hydroxide ions is greater. Thus, $[TMIm]^+$ is least stable in an alkaline environment compared to $[DMIIm]^+$ and $[DMBIm]^+$. $[DMIIm]^+$ exhibited the highest LUMO energy; therefore, it is considered the stable cationic head in an alkaline environment. Park and team[150] conducted molecular dynamics simulations to analyze the impact of functional groups on hydrocarbon anion-exchange membranes. The investigation focused on ethyl imidazolium (EI) and quaternary ammonium (QA) functional groups within the poly(arylene ether sulfone) (PES) backbone. The study involved calculating the mean-square displacement of OH^- ions in both hydrated EI-PES and QA-PES systems at two distinct temperatures, 293 K and 353 K. Notably, the mean square displacement was observed to be highest in hydrated EI-PES at 353 K, signifying that EI-PES exhibited the highest conductivity among the examined groups. Moreover, through their analysis from radial distribution functions, it was found that EI-PES has greater alkaline stability compared to QA-PES. Takaba *et al.*[151] carried out modelling of poly(arylene ether sulfone ketone)-based membranes containing fluorenyl groups and showed that OH^- ion transport is mainly governed *via* surface diffusion of $H_3O_2^-$. Zhang *et al.*[152] analyzed three different types of AEMs based on poly(ether sulfone) (QAPIPPES), poly(phenylene oxide) (PI-PPO), and poly(aryl piperidinium) (PAP-BP). Through MD simulation, it was found PAP-BP showed a lower SR and efficient transportation of hydroxide ions (see Fig. 8). The obtained outcomes were also closely aligned with the experimental findings. Sepehr and research group[153] explored the hydrated morphology and microscopic arrangement of a triblock copolymer, polystyrene-*b*-poly(ethylene-*co*-butylene)-*b*-polystyrene (SEBS), with alkyl-substituted quaternary ammonium cationic functional groups. This investigation employed Dissipative Particle Dynamics (DPD) simulation to gain insights into the molecular morphology. The conclusion drawn was that the membrane's morphology was influenced by the degree of hydration. Zadok *et al.*[154] demonstrated the dominance of the hydroxide-paired structure over the conventional hydrated structure of hydroxide ions around the ammonium cations of AEMs and found a stable two-hydroxide ion-paired structure as a complex with water/ammonium groups.

Zelovich *et al.*[155] investigated the effect of temperature on hydroxide ion diffusion, using quaternary trimethylammonium ions as a functional group, computationally using *ab initio* molecular dynamics (AIMD) methods as well as experimentally using ^1H pulsed field gradient (PFG) nuclear magnetic resonance (NMR). For their theoretical investigation, a graphene bilayer served as the polymer backbone, and to validate their theoretical predictions, polysulfone (PSU)-based AEMs with TMA were utilized in their experimental analysis. In their examination, a notable increase in the diffusion of hydroxide ions at temperatures exceeding 400 K was observed. Furthermore, an unusual and distinct pattern in hydroxide ion diffusivity was detected. A kink around 350–400 K was observed, indicating that it is possible to achieve enhanced hydroxide ion diffusion at temperatures above the local minimum of the kink.

Table 3 Hydroxide ion conductivity attained using different pendant subgroups (hydration level is given by λ)

Polymer backbone with pendant subgroups	OH^- conductivity (mS cm^{-1})	IEC (mmol g^{-1}	Water uptake (%)	Tensile strength (MPa)	λ	Ref.
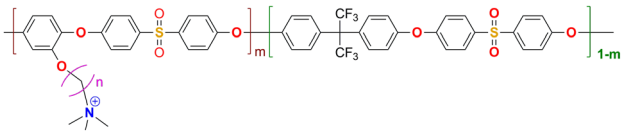	62.7 at 80 °C	1.48	77.5	9.2 ± 1.9	29.1	Lin *et al.*[132]
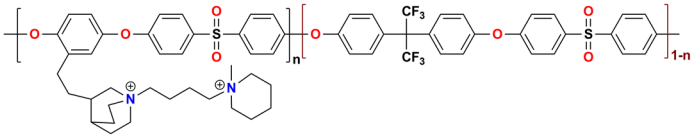	88 at 80 °C	1.35	53.83	47	23	Patil *et al.*[133]
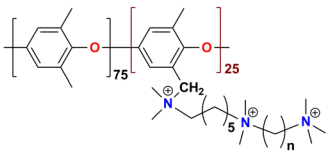	99 at 80 °C	2.87	189 ± 5	—	34	Zhu *et al.*[134]
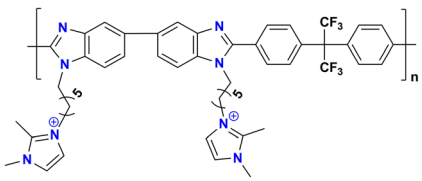	63.4 at 80 °C	2.09	36.9 ± 3.7	13 ± 1.4	—	Lin *et al.*[135]
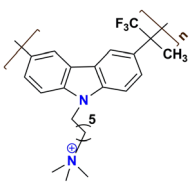	125 at 70 °C	2.31	76	—	—	Cha *et al.*[136]
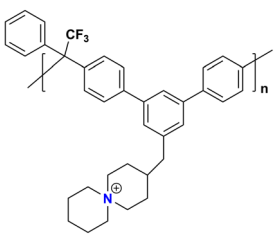	51 at 80 °C	1.57	54	—	17	Pham *et al.*[137]
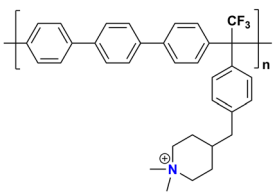	146 at 80 °C	1.73	103	—	30	Pham *et al.*[137]
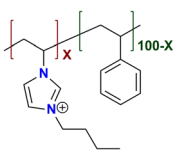	89.7 at 60 °C	1.65	101 ± 5.2	15.5	34	Park *et al.*[138]
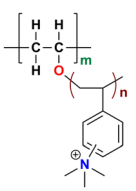	145 at 80 °C	2.87	104 ± 9	30	20 ± 2	Wang *et al.*[139]

Table 3 (*continued*)

Polymer backbone with pendant subgroups	OH^- conductivity (mS cm^{-1})	IEC (mmol g^{-1})	Water uptake (%)	Tensile strength (MPa)	λ	Ref.
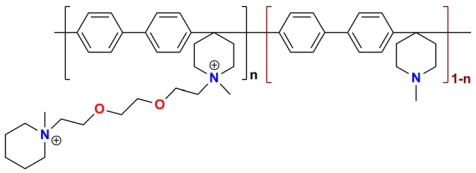	106 at 80 °C	1.93	46.1	7.4	—	Zhang *et al.*[140]
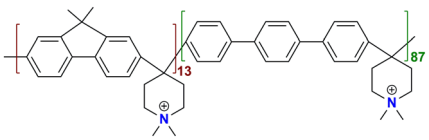	163 at 80 °C	2.82	73	71	—	Chen *et al.*[141]
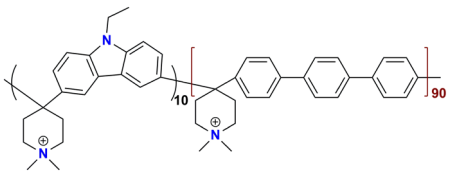	204.8 at 90 °C	2.76	54.9	52.2 ± 1.6	—	Yuan *et al.*[142]
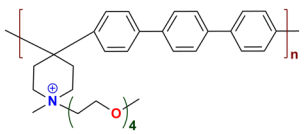	104.2 at 80 °C	1.47	101	60	—	Liu *et al.*[143]
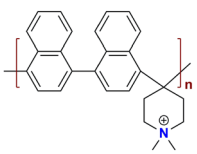	135.25 at 80 °C	2.29–2.60	38.5	35	3.48–8.25	Gao *et al.*[144]
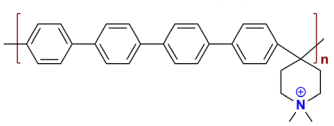	109.12 at 80 °C	2.29–2.60	15	60	3.48–8.25	Gao *et al.*[144]
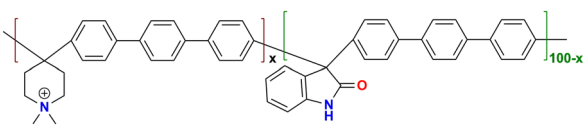	128.9 at 80 °C	2.52	86.9	29.2	8.7	Hu *et al.*[145]
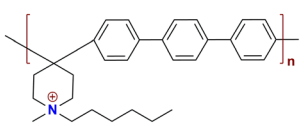	86.6 at 80 °C	2.34	20	57	—	Liu *et al.*[143]
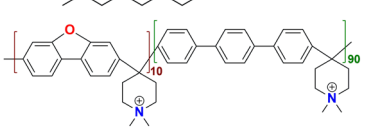	144.7 at 80 °C	2.82	169.9	42	—	Jeong *et al.*[146]

Pan and co-workers[156] analyzed an olefinic-based anion-exchange membrane with different types of mono and di-cationic functional groups, both experimentally and theoretically. From their investigation, it was concluded that di-cationic functional groups exhibit better stability and conductivity, a smaller swelling ratio and better water uptake. Lee *et al.*[157] employed DPD mesoscale simulations to examine PPO with TMA cations under varying hydration levels and IEC. The simulation results indicated that higher hydration levels led to increased water and anion diffusivity, aligning with experimental findings. Additionally, the research revealed that elongating the hydrophobic alkyl chain augmented the enhanced phase-separation between hydrophilic and hydrophobic domains. Luo and co-workers[158] examined the water-induced structure of SEBS with quaternary ammonium through mesoscale DPD calculations. Their study revealed that elevating the hydration level changed the structure from perforated and interconnected lamellae to a perfect lamellae.

Li *et al.*[159] performed molecular dynamics simulations to understand the effect of side-chain position on hydroxide transport. Their research groups developed three types of

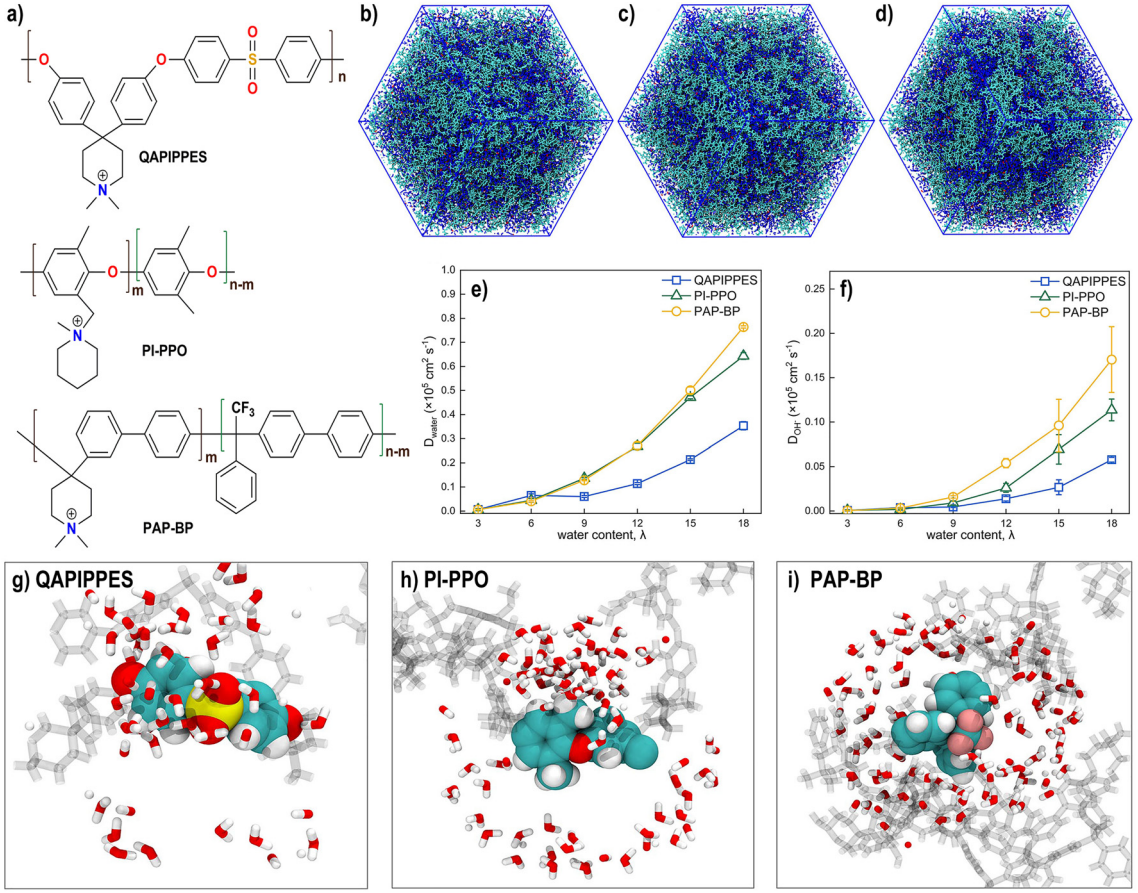

Fig. 8 (a) Polymer structures; snapshots of systems (b) QAPIPPES, (c) PI-PPO, and (d) PAP-BP respectively at λ = 18; diffusion coefficients of (e) water molecules and (f) hydroxide ions in AEMs; MD snapshots of backbone segments with neighbouring water molecules and hydroxides in (g) QAPIPPES, (h) PI-PPO, and (i) PAP-BP. Panels (b)–(i) have been adapted/reproduced from Zhang *et al.*[152] with permission from Elsevier, copyright 2022.

long-side-chain poly(arylene indole piperidinium) anion-exchange membranes (AEMs): tadpole-chain configuration (t-PITPC10), pendant-chain arrangement (p-PITPC10), and a configuration where side chains are connected to the backbone but separated from the cationic groups (a-PITPC10). The simulation outcomes revealed that among the three, a-PITPC10 exhibited greater efficacy in improving the transport of hydroxide ions (see Fig. 9). Kim and their research team[160] conducted molecular dynamics simulations to investigate how different functional groups affect the behavior of hydroxide ions in hydrated poly(ether ether ketone) (PEEK) with ammonium cationic heads. During the simulations, they systematically varied the concentration of functional groups, ranging from 0 to 40 mol%. Their findings indicated that as the amount of functional groups and water increased, the diffusion of ions also increased. However, they observed that when a large quantity of water was introduced into the simulation environment, it led to a lower polymer density and weakened connections between ionic sites. A combined study of DFT-based calculations and molecular dynamics simulations was conducted by Di Salvo and co-workers[161] to analyse the effect of IEC on diffusion of hydroxide ions in AEMs. The *ab initio* calculations accurately projected the water absorption levels at various IECs, aligning well with the experimental observations. The study identified a critical IEC range of 1.2–1.7 meq g^{-1}, within which the AEM experience excessive swelling.

Recently, Zelovich *et al.*[162] analyzed the impact of functional groups on the diffusion of hydroxide ions and water in anion-exchange membranes using *ab initio* molecular dynamics (AIMD) techniques. Two distinct functional groups, trimethyl alkyl ammonium (TMA) and imidazolium (IMI), were employed in the investigation. A graphene bilayer served as the polymer framework. Their findings revealed that hydroxide ion diffusion was similar for both functional groups when temperatures exceeded 400 K. However, when temperatures dropped below 350 K, the TMA functional group exhibited greater hydroxide ion diffusivity. Conversely, in the case of IMI, higher water diffusivity was observed across all temperature ranges. Enhanced water diffusivity reduces the risk of cathode dehydration. Sharma *et al.*[163] employed a molecular dynamics study using a quaternary ammonium functonalized Nafion membrane at varying hydration. The authors found a significant role of hydration in distinct inter-chain and intra-chain pendant group interactions with hydroxide ions. A coarse-grained molecular dynamics simulation was carried out by Chen and co-workers[164] to explore two PEEK-based AEMs containing different types of

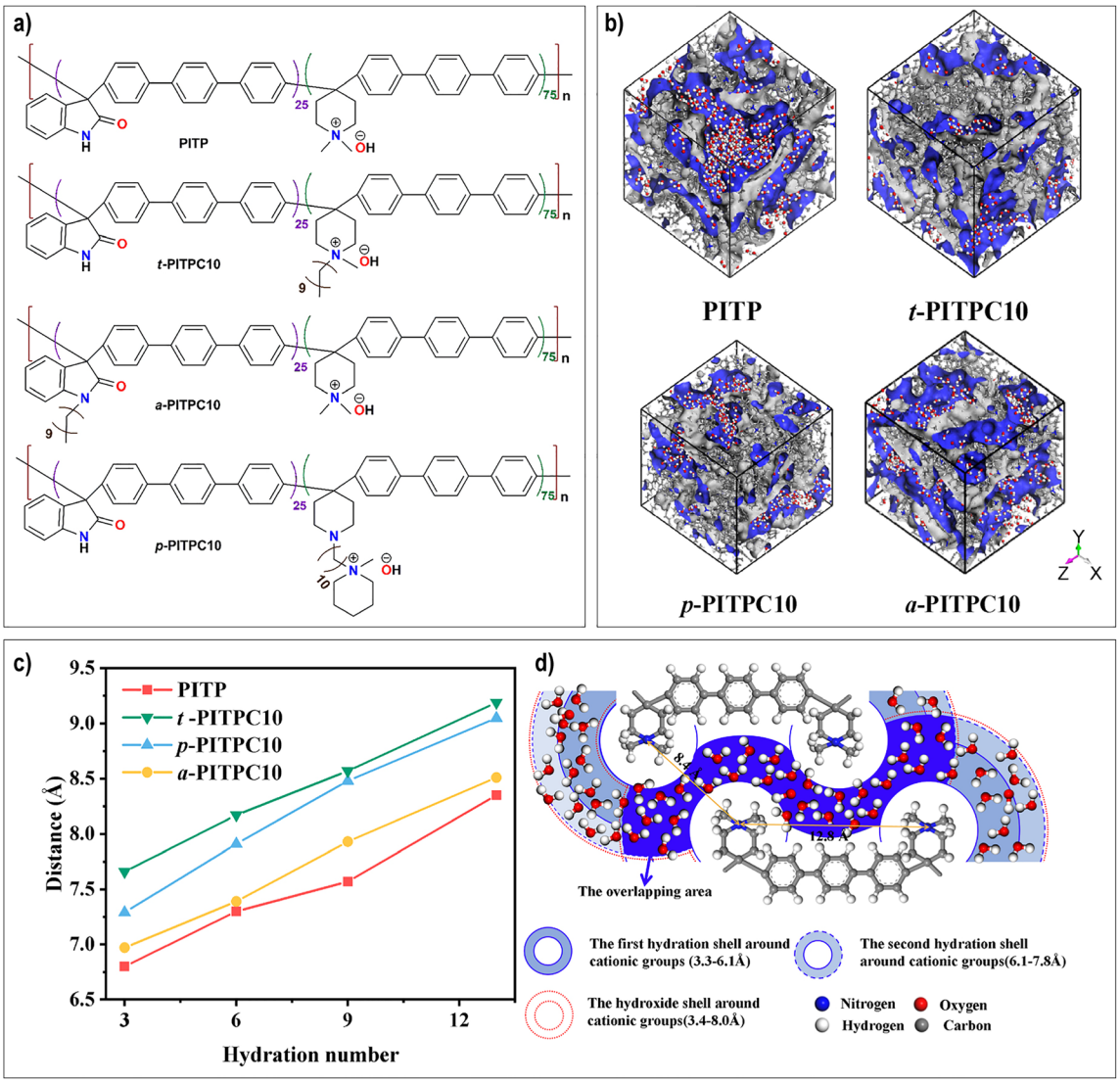

Fig. 9 (a) Chemical structures of poly(arylene indole piperidinium) AEMs: without a side chain (PITP), with a tadpole chain (t-PITPC10), with a pendant chain (p-PITPC10), and with side chains connected to the backbone separated from the cationic groups (a-PITPC10); (b) snapshots of ion transport channels in AEMs at λ = 13; (c) distances between the adjacent cationic groups in AEMs at different hydration numbers; and (d) schematic diagram of adjacent hydration shells in a-PITPC10 at λ = 13. Panels (b)–(d) have been adapted/reproduced from Li *et al.*[159] with permission from Elsevier, copyright 2023.

side chains: one containing single quaternary (SQ) and the other containing gemini quaternary (GQ) ammonium groups. The simulation results demonstrated enhanced ionic conductivity in the case of GQ. The improvement was attributed to an increase in IEC rather than the self-diffusion coefficient, as both SQ and GQ exhibited similar self-diffusion coefficients in the simulations. Additionally, the study revealed that more water molecules surrounded the OH^- groups for GQ, potentially contributing to its superior alkaline stability compared to SQ.

Ma and his research team[165] examined the impact of incorporating a polar cyano-group side chain in poly(biphenyl piperidine-trifluoroacetophenone)-based AEMs, both theoretically and experimentally. Their findings revealed that AEMs containing the polar cyano group exhibited favorable ionic conductivity, improved mechanical properties, clearer microphase separation structures, and lower SR and WU. Through molecular dynamics simulations and experimental analysis, they demonstrated that AEMs with cyano-group side chains managed to strike a balance between high ionic conductivity and dimensional stability, addressing the inherent trade-off challenge in AEMs.

Chen and team[166] investigated the effect of block size on hydroxide solvation and transportation in a diblock copolymer (PPO-*b*-PVBTMA). During their simulation, they kept the number of PVBTMA ions, hydroxide ions, and water molecules constant while increasing the PPO block count. Their findings revealed that an increase in the PPO block resulted in the constriction of water channels within the system. This constriction was supported by the reduction in the coordination number of water molecules around cationic groups and

hydroxide ions, leading to a decrease in the diffusion constants of both hydroxide ions and water molecules. A study analyzing the impact of high-temperature operation on AEMFCs was conducted by Yassin and team.[167] Using molecular studies, an increase in the AEMFC performance stability was found as the temperature increased from 45 °C up to 120 °C. Additionally, their findings indicated that when operating an AEMFC at a current density of 0.6 A cm^2, the degradation rate constant decreases as the temperature increases. In a separate research endeavor, Yassin and group[168] investigated the impact of membrane thickness on AEMFC fuel cells. They conducted a comprehensive study, combining theoretical analysis with experiments, focusing on commercially available FAA-3 AEMs with varying thicknesses, ranging from 5 to 50 micrometers (μm). The results revealed that reducing the thickness from 30 to 20 μm led to a moderate improvement in cell performance. However, a further reduction to 5 μm resulted in a significant enhancement in performance. Additionally, the researchers explored the influence of membrane thickness using two different cathode catalysts, Pt/C and Fe–N–C. In both cases, a decrease in membrane thickness led to an improvement in cell performance.

Sharma *et al.*[169] investigated poly(ether ether ketone) (PEEK)-based membranes, primarily focusing on PEEK functionalized with trimethylammonium. In addition to PEEK-TMA, variations in alkyl chains and different cationic functional groups were examined to understand their influence on membrane behavior. From a computational perspective, the work employed all-atom molecular dynamics simulations using the GAFF force field, with the TIP3P water model, implemented in GROMACS. The systems were equilibrated under the NPT ensemble, followed by annealing cycles and extended production runs. Different hydration levels (λ = 5–25) were considered to systematically study the effect of water content on membrane morphology and ion transport. Importantly, the computational predictions were supported by experimental validation. The simulated dry density (1220 ± 4.2 kg m^{-3}) showed less than 10% deviation from the reported experimental range (1260–1320 kg m^{-3}), indicating accurate structural packing in the model. Similarly, the predicted glass-transition temperature (T_g) of 440–448 K was in close agreement with the experimental range of 418–423 K, supporting the reliability of the simulation approach. Furthermore, Pu and Sun[170] investigated two AEMs containing piperidinium cationic head groups but different polymer backbones, a triphenyl-based backbone (QAPPT) and a quaterphenyl-based backbone (QAQPP) system. All-atom molecular dynamics simulations were performed using the OPLS/AA force field for the polymer chains, while the SPC/E water model was employed to describe water molecules.

To validate the reliability of their simulations, the authors first examined the dry-state membrane structure by calculating the IEC; the simulated IEC values were 2.80 mmol g^{-1} for QAPPT and 2.31 mmol g^{-1} for QAQPP, which showed close agreement with the corresponding experimental values of 2.6516 and 2.2922 mmol g^{-1}, respectively. Beyond the dry state, the fully hydrated membrane structures were also assessed through swelling behavior. The calculated volume expansion from dry to fully hydrated conditions was 18.1% for QAPPT and 0.6% for QAQPP. These trends matched experimental swelling degree (SD) values of 9.5% for QAPPT and 2.3% for QAQPP.

7 Future perspectives and development trends of AEMs

Recent progress in the AEM field underscores that structural modification of the polymer and cationic head, as well as the arrangement of its hydrophilic and hydrophobic domain, plays a decisive role in enhancing ion transport, dimensional stability, and alkaline durability. Significant improvements have been achieved through the development of diverse polymer backbones and pendant cationic groups, along with innovative architectures such as block, comb-shaped, grafted, branched, and cross-linked systems. These approaches not only protect the integrity of cationic head-groups under highly alkaline conditions but also promote the formation of well-organized ionic domains that facilitate efficient hydroxide transport while limiting excessive swelling. Despite these advancements, several challenges remain before AEM-based technologies can be fully commercialized, such as:

- **Polymer and cation design**: further improvement is still needed in the polymer backbone and the attached cationic groups so that the membrane can survive longer under strong alkaline conditions.[171] By carefully modifying the main polymer structure and the side cationic groups, the overall alkaline durability can be increased. One important approach is to design cations that are sterically protected. In addition, removing or avoiding β-hydrogen atoms in the cation structure can help prevent common degradation reactions such as elimination and nucleophilic substitution. Researchers are also studying multi-cationic and dicationic functional groups, where more than one positive charge is present, because these groups can provide better chemical stability and ionic conductivity.
- **Backbone rigidity**: using an ether-free, fully aromatic backbone can significantly improve stability under strong alkaline conditions.[172,173] A rigid backbone helps reduce segmental motion of the polymer chains, which minimizes water-induced swelling. However, if the backbone becomes too rigid, ion movement inside the membrane can slow down, which lowers conductivity. Therefore, it is important to maintain a proper balance between mechanical strength and chain flexibility to allow efficient ion transport. Moreover, poly(aryl piperidinium)-type backbones consistently provide improved alkaline durability due to elimination of benzylic sites, particularly when paired with sterically protected cyclic ammonium cations.
- **Water management and hydration structure**: hydroxide ion transport inside the membrane mainly depends on how water molecules surround the ions within the membrane structure.[174] If the membrane absorbs too much water, it causes swelling. On the other hand, if there is not enough water, the continuous pathways needed for OH^- movement get disturbed, and ion transport becomes difficult. Therefore,

future membrane designs should focus on creating well-controlled and confined water channels that maintain a continuous pathway while avoiding excessive swelling.

• **Role of Free Volume and chain dynamics**: the free volume present inside a polymer plays an important role in controlling how water molecules move and how easily hydroxide ions can travel through the membrane.[175] When the free volume is properly controlled, it can reduce the energy required for ion transport and improve conductivity. However, if the free volume becomes too high, it weakens the structure and reduces stability. The density of chain entanglement in the polymer also matters, as it influences mechanical strength. Side-chain engineering enhances conductivity through phase separation but often increases swelling unless constrained by crosslinking or hydrogen-bonding networks. For developing next-generation membranes, it will be very important to carefully evaluate these parameters.

• **Linking AEM to electrochemical performance**: to clearly understand how molecular design affects real device performance, membrane properties such as ionic conductivity, swelling behaviour, mechanical strength, and alkaline stability must be tested under practical operating conditions, including high current density, peak power density, elevated temperature, and varying humidity.[176] Therefore, future studies may correlate molecular degradation mechanisms with voltage decay and performance loss. The stability rankings are shown to depend strongly on testing temperature, hydroxide concentration, and hydration state and need to be accommodated in rational design.

8 Conclusions

This review systematically highlighted the notable progress achieved in the domain of AEMs, particularly polymer backbone and pendant group developments in AEMFCs. A thorough approach was adopted in accentuating a range of efforts encompassing experimental and molecular studies. To counter the adverse impact of the highly alkaline environment on the cationic functional group's stability, researchers have innovatively devised various membrane structures, including block, comb, and graft polymers. The innovative strategy of random or block polymers serves dual purpose: (a) safeguarding the integrity of the cationic head, and (b) promoting the formation of a phase-separated membrane morphology. The optimization of structural characteristics through various cationic heads has made a significant impact on improvement of hydroxide ion conductivity and durability. Other strategies encompass crosslinking, polymer chain branching, and the integration of multi-cationic functional groups as pendant moieties. This review covers diverse membrane synthesis methodologies, encompassing distinct polymer backbones and cationic functional groups. AEM success for the goal of future decarbanization[177] largely depends on integration of ionomer performance, durability and effective electro-catalysts at commercially feasible cost.[178,179] It is noteworthy that increasing the side-chain length enhances conductivity but can also lead to greater swelling. In contrast, cross-linking enhances dimensional stability, though it may decrease molecular mobility.

In addition, the assessment addresses the capability of computational methodologies in scrutinizing AEM properties. DFT methods have demonstrated their utility in evaluating the stability of the cationic head connected to the polymer backbone. Molecular dynamics simulations have yielded insights into the diffusion of hydroxide ions within the membrane. Computational techniques have further enabled the analysis of hydroxide ion conductivity, WU, SR, and various other membrane properties. Mesoscale calculations using DPD have been used in investigating the membrane morphology. Despite the remarkable advancements witnessed in recent years within the AEM field, certain challenges remain. Tackling aspects such as efficient water management, membrane stability under elevated temperatures, and the identification of optimal operating conditions is pivotal for unlocking the full potential of AEMFCs. With improved technology and machine-learning methods, the roles of free volume[180] in the polymer matrix and chain entanglements[175,181] need to be explored in detail for future generation AEMs. In summary, a decisive path through AEMs may certainly come true and we may get closer to a fossil-fuel-independent future with green and renewable energy.

Author contributions

PS and APS contributed to writing and review-editing. APS administrated the project and helped in the funding acquisition, analysis and discussion.

Conflicts of interest

There are no conflicts to declare.

Abbreviations

AEMFC	Anion-exchange-membrane fuel cell
PEMFC	Proton-exchange-membrane fuel cell
AEM	Anion-exchange membrane
PPO	Polyphenyleneoxide
TMA	Trimethyl ammonium
WU	Water uptake
SR	Swelling ratio
QAPIPPES	Quaternary-ammonium-based piperidinium poly ether sulfone
PAP-BP	Biphenyl poly(aryl piperidinium)
PI-PPO	Piperidinium polyphenyleneoxide
BMP	1-(6-Bromohexyl)-1-methylpiperidinium bromide
DFT	Density functional theory
DPD	Dissipative particle dynamics
Dha	Dihydroxyterephthalaldehyde
TGCl	Triaminoguanidinium chloride
IEC	Ion exchange capacity

Data availability

No new data were generated or analyzed during this review. All data discussed in this manuscript are derived from previously published studies, which are cited in the reference list.

Acknowledgements

PS thanks the Council of Scientific and Industrial Research, New Delhi for a Junior Research Fellowship (09/1256(19767)/2024-EMR-I). APS acknowledges the 'Anusandhan National Research Foundation (ANRF)', Govt. of India for SERB – CRG/2022/001938 Research Grant.

Notes and references

1 B. G. Pollet, S. S. Kocha and I. Staffell, *Curr. Opin. Electrochem.*, 2019, **16**, 90–95.
2 D. Li, A. R. Motz, C. Bae, C. Fujimoto, G. Yang, F.-Y. Zhang, K. E. Ayers and Y. S. Kim, *Energy Environ. Sci.*, 2021, **14**, 3393–3419.
3 G. Das, J.-H. Choi, P. K. T. Nguyen, D.-J. Kim and Y. S. Yoon, *Polymers*, 2022, **14**, 1197.
4 A. Arshad, H. M. Ali, A. Habib, M. A. Bashir, M. Jabbal and Y. Yan, *Therm. Sci. Eng. Prog.*, 2019, **9**, 308–321.
5 M. A. Abdelkareem, K. Elsaid, T. Wilberforce, M. Kamil, E. T. Sayed and A. Olabi, *Sci. Total Environ*, 2021, **752**, 141803.
6 N. A. A. Qasem and G. A. Q. Abdulrahman, *Int. J. Energy Res.*, 2024, **2024**, 7271748.
7 C. Kalyvas, A. Kucernak, D. Brett, G. Hinds, S. Atkins and N. Brandon, *WENE*, 2014, **3**, 254–275.
8 E. Qu, X. Hao, M. Xiao, D. Han, S. Huang, Z. Huang, S. Wang and Y. Meng, *J. Power Sources*, 2022, **533**, 231386.
9 A. T. Hamada, M. F. Orhan and A. M. Kannan, *Energy Rep.*, 2023, **9**, 6396–6418.
10 M. Hren, M. Božic, D. Fakin, K. S. Kleinschek and S. Gorgieva, *Sustainable Energy Fuels*, 2021, **5**, 604–637.
11 N. Shaari, S. K. Kamarudin, R. Bahru, S. H. Osman and N. A. I. Md Ishak, *Int. J. Energy Res.*, 2021, **45**, 6644–6688.
12 J. Rosen, T. Geary, A. Hilmi, R. Blanco-Gutierrez, C.-Y. Yuh, C. S. Pereira, L. Han, R. A. Johnson, C. A. Willman and H. Ghezel-Ayagh, *et al.*, *J. Electrochem. Soc.*, 2020, **167**, 064505.
13 S. Z. Golkhatmi, M. I. Asghar and P. D. Lund, *Renewable Sustainable Energy Rev.*, 2022, **161**, 112339.
14 S. P. Jiang, Q. Li, S. P. Jiang and Q. Li, *Introduction to Fuel Cells: Electrochemistry and Materials*, 2022, pp. 649–671.
15 F. M. L. Figueiredo and F. M. B. Marques, *WENE*, 2013, **2**, 52–72.
16 L. Dubau, L. Castanheira, F. Maillard, M. Chatenet, O. Lottin, G. Maranzana, J. Dillet, A. Lamibrac, J.-C. Perrin, E. Moukheiber, A. ElKaddouri, G. De Moor, C. Bas, L. Flandin and N. Caqu, *WIREs Energy Environ.*, 2014, **3**, 540–560.
17 N. Sazali, W. N. Wan Salleh, A. S. Jamaludin and M. N. Mhd Razali, *Membranes*, 2020, **10**, 99.
18 A. P. Sunda, S. Singh, S. Yadav and R. K. Singh, *Chem. Phys. Chem.*, 2023, **24**, e202300104.
19 R. Vedarajan, R. Balaji and K. Ramya, *Wiley Interdiscip. Rev.:Energy Environ.*, 2023, e466.
20 N. Alonso-Vante and V. Di Noto, *Electrocatalysis for Membrane Fuel Cells: Methods, Modeling,and Applications*, John Wiley & Sons, 2023.
21 H. Lei, X. Yang, Z. Chen, D. Rawach, L. Du, Z. Liang, D.-S. Li, G. Zhang, A. C. Tavares and S. Sun, *Adv. Mater.*, 2025, **37**, 2410106.
22 K. Yassin and D. R. Dekel, *Front. Membr. Sci. Technol.*, 2025, **4**, 1691096.
23 L. Liu, H. Ma, M. Khan and B. S. Hsiao, *Membranes*, 2024, **14**, 85.
24 M. Warshay and P. R. Prokopius, *The Fuel Cell in Space: Yesterday, Today and Tomorrow*, NASA Technical Memorandum NASA-TM-102366, 1989, https://ntrs.nasa.gov/citations/19900002488.
25 Y.-J. Wang, J. Qiao, R. Baker and J. Zhang, *Chem. Soc. Rev.*, 2013, **42**, 5768–5787.
26 M. Muhyuddin, C. Santoro, L. Osmieri, V. C. A. Ficca, A. Friedman, K. Yassin, G. Pagot, E. Negro, A. Konovalova, G. Lindquist, L. Twight, M. Kwak, E. Berretti, V. D. Noto, F. Jaouen, L. Elbaz, D. R. Dekel, P. Mustarelli, S. W. Boettcher, A. Lavacchi and P. Atanassov, *Chem. Rev.*, 2025, **125**, 6906–6976.
27 E. Tomasino, P. Scardi and N. Ataollahi, *MRS Energy Sustain.*, 2025, **12**, 203–222.
28 Z. Li, X. He, Z. Jiang, Y. Yin, B. Zhang, G. He, Z. Tong, H. Wu and K. Jiao, *Electrochim. Acta*, 2017, **240**, 486–494.
29 E. J. Park, P. Jannasch, K. Miyatake, C. Bae, K. Noonan, C. Fujimoto, S. Holdcroft, J. R. Varcoe, D. Henkensmeier, M. D. Guiver and Y. S. Kim, *Chem. Soc. Rev.*, 2024, **53**, 5704–5780.
30 J. Miyake and K. Miyatake, *Sustainable Energy Fuels*, 2019, **3**, 1916–1928.
31 R. Vinodh, S. S. Kalanur, S. K. Natarajan and B. G. Pollet, *Polymers*, 2023, **15**, 2144.
32 D. Henkensmeier, M. Najibah, C. Harms, J. Žitka, J. Hnát and K. Bouzek, *J. Electrochem. Energy Con. Stor.*, 2021, **18**, 024001.
33 A. P. Sunda and J. C. Bose, *J. Eng. Technol. Sci.*, 2025, **1**, 1–14.
34 Z. Wang, G. Sun, N. H. C. Lewis, M. Mandal, A. Sharma, M. Kim, J. M. Montes de Oca, K. Wang, A. Taggart, A. B. Martinson, P. A. Kohl, A. Tokmakoff, S. N. Patel, P. F. Nealey and J. J. de Pablo, *Nat. Commun.*, 2025, **16**, 1099.
35 N. Du, C. Roy, R. Peach, M. Turnbull, S. Thiele and C. Bock, *Chem. Rev.*, 2022, **122**, 11830–11895.
36 J. Pan, J. Han, L. Zhu and M. A. Hickner, *Chem. Mater.*, 2017, **29**, 5321–5330.
37 T. Nemeth, T. Nauser and L. Gubler, *ChemSusChem*, 2022, **15**, e202201571.

38 A. M. Samsudin, M. Bodner and V. Hacker, *Polymers*, 2022, **14**, 3565.
39 A. M. Barnes, Y. Du, W. Zhang, S. Seifert, S. K. Buratto and E. B. Coughlin, *Macromolecules*, 2019, **52**, 6097–6106.
40 J. Ye, S. Yu, C. Zheng, T. Sun, J. Liu and H. Li, *Chem. Eng. J.*, 2022, **427**, 131413.
41 M. A. Hossain, H. Jang, S. C. Sutradhar, J. Ha, J. Yoo, C. Lee, S. Lee and W. Kim, *Int. J. Hydrogen Energy*, 2016, **41**, 10458–10465.
42 K. Wang, Z. Zhang, S. Li, H. Zhang, N. Yue, J. Pang and Z. Jiang, *ACS Appl. Mater. Interfaces*, 2021, **13**, 23547–23557.
43 U. Salma and N. Shalahin, *Results Mater.*, 2023, 100366.
44 J. Ren, J. Xu, M. Ju, X. Chen, P. Zhao, L. Meng, J. Lei and Z. Wang, *Adv. Powder Mater.*, 2022, **1**, 100017.
45 Z. Xu, S. Delgado, V. Atanasov, T. Morawietz, A. S. Gago and K. A. Friedrich, *Membranes*, 2023, **13**, 328.
46 W. Tang, Y. Yang, X. Liu, J. Dong, H. Li and J. Yang, *Electrochim. Acta*, 2021, **391**, 138919.
47 S. Bonizzoni, D. Stucchi, T. Caielli, E. Sediva, M. Mauri and P. Mustarelli, *ChemElectroChem*, 2023, **10**, e202201077.
48 D. Pan, P. M. Bakvand, T. H. Pham and P. Jannasch, *J. Mater. Chem. A*, 2022, **10**, 16478–16489.
49 E. Cabukoglu, G. Georges, L. Kung, G. Pareschi and K. Boulouchos, *Transp. Res. D: Transp. Environ.*, 2019, **70**, 35–48.
50 B. Pivovar, *Nat. Catal.*, 2019, **2**, 562–565.
51 B. E. Anley, Y. W. Ahmed, A. Yusuf, A. Candra, S. L. Kitaw, T.-Y. Wu, C.-C. Huang, J.-S. Wang, D. Thankachan, M. H. Khan, Y.-T. Cheng, C.-H. Wang and H.-C. Tsai, *ACS Appl. Mater. Interfaces*, 2026, **18**, 6687–6700.
52 N. Chen, H. H. Wang, S. P. Kim, H. M. Kim, W. H. Lee, C. Hu, J. Y. Bae, E. S. Sim, Y.-C. Chung, J.-H. Jang, S. J. Yoo, Y. Zhuang and Y. M. Lee, *Nat. Commun.*, 2021, **12**, 2367.
53 Z. Yu, W. T. Gao, Y. J. Liu, Q. G. Zhang, A. M. Zhu and Q. L. Liu, *J. Colloid Interface Sci.*, 2023, **651**, 404–414.
54 S. C. Ramarez and R. R. Paz, *New Trends in Ion Exchange Studies*, IntechOpen, London, 2018, ch. 4.
55 B. Cermenek, J. Ranninger and V. Hacker, *Ethanol*, Elsevier, 2019, pp. 383–405.
56 F. Foglia, Q. Berrod, A. J. Clancy, K. Smith, G. Gebel, V. G. Sakai, M. Appel, J.-M. Zanotti, M. Tyagi, N. Mahmoudi, T. S. Miller, J. R. Varcoe, A. P. Periasamy, D. J. L. Brett, P. R. Shearing, S. Lyonnard and P. F. McMillan, *Nat. Mater.*, 2022, **21**, 555–563.
57 Z. Sun, B. Lin and F. Yan, *ChemSusChem*, 2018, **11**, 58–70.
58 F. Li, S. H. Chan and Z. Tu, *Chem. Rec.*, 2023, e202300067.
59 S. Gottesfeld, D. R. Dekel, M. Page, C. Bae, Y. Yan, P. Zelenay and Y. S. Kim, *J. Power Sources*, 2018, **375**, 170–184.
60 R. Kingsbury, K. Bruning, S. Zhu, S. Flotron, C. Miller and O. Coronell, *Ind. Eng. Chem. Res.*, 2019, **58**, 18663–18674.
61 E. Drioli and L. Giorno, *Encyclopedia of membranes*, Springer, 2018.
62 F. Karas, J. Hnát, M. Paidar, J. Schauer and K. Bouzek, *Int. J. Hydrogen Energy*, 2014, **39**, 5054–5062.
63 B. Yang and Z. Cunman, *Chem. Eng. J.*, 2023, **457**, 141094.
64 F. Xu, Y. Su and B. Lin, *Front. Mater.*, 2020, **7**, 4.
65 A. L. Frischknecht, P. J. int Veld, I. V. Kolesnichenko, D. J. Arnot and T. N. Lambert, *ACS Appl. Polym. Mater.*, 2022, **4**, 2470–2480.
66 J. M. Clary, L. Wang, Y. Yan, A. L. Frischknecht and D. Vigil-Fowler, *J. Membr. Sci.*, 2025, **717**, 123517.
67 A. Barnett, J. Lu and V. Molinero, *J. Phys. Chem. C*, 2021, **125**, 27703–27713.
68 W. F. Drayer, E. M. Duan, J. C. Johnson, K. I. Winey and A. L. Frischknecht, *Macromolecules*, 2025, **58**, 10017–10025.
69 F. Razmjooei, A. Farooqui, R. Reissner, A. S. Gago, S. A. Ansar and K. A. Friedrich, *ChemElectroChem*, 2020, **7**, 3951–3960.
70 R. Gutru, Z. Turtayeva, F. Xu, G. Maranzana, B. Vigolo and A. Desforges, *Int. J. Hydrogen Energy*, 2020, **45**, 19642–19663.
71 K. Otsuji, Y. Shirase, T. Asakawa, N. Yokota, K. Nagase, W. Xu, P. Song, S. Wang, D. A. Tryk and K. Kakinuma, *et al.*, *J. Power Sources*, 2022, **522**, 230997.
72 Y. Zheng, U. Ash, R. P. Pandey, A. G. Ozioko, J. Ponce-Gonzalez, M. Handl, T. Weissbach, J. R. Varcoe, S. Holdcroft, M. W. Liberatore, R. Hiesgen and D. R. Dekel, *Macromolecules*, 2018, **51**, 3264–3278.
73 Z. Xu, L. Wan, Y. Liao, P. Wang, K. Liu and B. Wang, *J. Mater. Chem. A*, 2021, **9**, 23485–23496.
74 C. G. Arges, V. K. Ramani and P. N. Pintauro, *Electrochem. Soc. Interface*, 2010, **19**, 31.
75 W. E. Mustain, M. Chatenet, M. Page and Y. S. Kim, *Energy Environ. Sci.*, 2020, **13**, 2805–2838.
76 B. Lee, D. Yun, J.-S. Lee, C. H. Park and T.-H. Kim, *J. Phys. Chem. C*, 2019, **123**, 13508–13518.
77 P. Sgarbossa, G. Crivellaro, F. Lanero, G. Pagot, A. R. Alvi, E. Negro, K. Vezzù and V. Di Noto, *Electrocatalysis for Membrane Fuel Cells: Methods, Modeling and Applications*, 2023, pp. 227–285.
78 D. Li, E. J. Park, W. Zhu, Q. Shi, Y. Zhou, H. Tian, Y. Lin, A. Serov, B. Zulevi, E. D. Baca, C. Fujimoto, H. T. Chung and Y. S. Kim, *Nat. Energy*, 2020, **5**, 378–385.
79 R. Yu, H. Yang, X. Yu, J. Cheng, Y. Tan and X. Wang, *Int. J. Hydrogen Energy*, 2024, **50**, 582–604.
80 X. Su, L. Gao, L. Hu, N. A. Qaisrani, X. Yan, W. Zhang, X. Jiang, X. Ruan and G. He, *J. Membr. Sci.*, 2019, **581**, 283–292.
81 K. Min, J. E. Chae, Y. Lee, H.-J. Kim and T.-H. Kim, *J. Membr. Sci.*, 2022, **653**, 120487.
82 Y. Yuan, X. Du, H. Zhang, H. Wang and Z. Wang, *J. Membr. Sci.*, 2022, **642**, 119986.
83 D. R. Dekel, M. Amar, S. Willdorf, M. Kosa, S. Dhara and C. E. Diesendruck, *Chem. Mater.*, 2017, **29**, 4425–4431.
84 N. Gjineci, S. Aharonovich, D. R. Dekel and C. E. Diesendruck, *ACS Appl. Mater. Interfaces*, 2020, **12**, 49617–49625.
85 J. Muller, A. Zhegur, U. Krewer, J. R. Varcoe and D. R. Dekel, *ACS Mater. Lett.*, 2020, **2**, 168–173.
86 I. Agami, N. Gjineci, S. Li, S. Srebnik, D. R. Dekel and C. E. Diesendruck, *ACS Appl. Polym. Mater.*, 2022, **4**, 9250–9256.

87 S. Willdorf-Cohen, A. Zhegur-Khais, J. Ponce-Gonzalez, S. Bsoul-Haj, J. R. Varcoe, C. E. Diesendruck and D. R. Dekel, *ACS Appl. Energy Mater.*, 2023, **6**, 1085–1092.
88 K. Aggarwal, N. Gjineci, A. Kaushansky, S. Bsoul, J. C. Douglin, S. Li, I. Salam, S. Aharonovich, J. R. Varcoe, D. R. Dekel and C. E. Diesendruck, *ACS Mater. Au*, 2022, **2**, 367–373.
89 T. Wang, D. Chen, C. Wang, H. Wei and Y. Ding, *Adv. Funct. Mater.*, 2025, **35**, 2422504.
90 Q. Liu, J. Han, B. Liu, Y. Wang, Y. Pang, T. Mu, K. Dong and C. Zhao, *J. Membr. Sci.*, 2025, **734**, 124480.
91 T. Wang, Y. Zhao, S. Wang, S. Cheng, S. Yang, H. Wei and Y. Ding, *J. Power Sources*, 2023, **557**, 232590.
92 J. Li, C. Liu, J. Ge, W. Xing and J. Zhu, *Chem. – Eur. J.*, 2023, **29**, e202203173.
93 N. Chen, J. H. Park, C. Hu, H. H. Wang, H. M. Kim, N. Y. Kang and Y. M. Lee, *J. Mater. Chem. A*, 2022, **10**, 3678–3687.
94 M. Guo, T. Ban, Y. Wang, X. Wang and X. Zhu, *J. Colloid Interface Sci.*, 2023, **638**, 349–362.
95 A. Das, B. Sana, R. Bhattacharyya, P. Chandra Ghosh and T. Jana, *ACS Appl. Polym. Mater.*, 2022, **4**, 1523–1534.
96 Z. Peng, Z. Ren, S. Chen, Y. Zhao, P. Jannasch and J. Yang, *Int. J. Hydrogen Energy*, 2025, **188**, 151884.
97 B. Motealleh, Z. Liu, R. I. Masel, J. P. Sculley, Z. Richard Ni and L. Meroueh, *Int. J. Hydrogen Energy*, 2021, **46**, 3379–3386.
98 S. Maurya, S.-H. Shin, Y. Kim and S.-H. Moon, *RSC Adv.*, 2015, **5**, 37206–37230.
99 A. M. Samsudin and V. Hacker, *Polymers*, 2019, **11**, 1399.
100 F. Wang, C. Li, J. Sang, Y. Cui and H. Zhu, *Int. J. Hydrogen Energy*, 2021, **46**, 36301–36313.
101 L. Wang, M. Bellini, H. A. Miller and J. R. Varcoe, *J. Mater. Chem. A*, 2018, **6**, 15404–15412.
102 A. L. G. Biancolli, S. Bsoul-Haj, J. C. Douglin, A. S. Barbosa, R. R. de Sousa Jr, O. Rodrigues Jr, A. J. Lanfredi, D. R. Dekel and E. I. Santiago, *J. Membr. Sci.*, 2022, **641**, 119879.
103 A. L. G. Biancolli, B. Chen, A. S. Menandro, F. C. Fonseca, E. I. Santiago and S. Holdcroft, *J. Mater. Chem. A*, 2024, **12**, 21442–21454.
104 W. You, K. J. Noonan and G. W. Coates, *Prog. Polym. Sci.*, 2020, **100**, 101177.
105 W. You, K. M. Hugar and G. W. Coates, *Macromolecules*, 2018, **51**, 3212–3218.
106 Y. Chen, M. M. Abdellatif and K. Nomura, *Tetrahedron*, 2018, **74**, 619–643.
107 Z. He, G. Wang, C. Wang, L. Guo, R. Wei, G. Song, D. Pan, R. Das, N. Naik and Z. Hu, *et al.*, *Polym. Rev.*, 2021, **61**, 689–713.
108 A. K. Singh, S. Kumar, M. Bhushan and V. K. Shahi, *Sep. Purif. Technol.*, 2020, **234**, 116078.
109 R. Lv, Z. Peng, Y. Wu, M. M. Gomaa and J. Yang, *J. Membr. Sci.*, 2026, **742**, 125120.
110 Q. Wang, T. Wei, Z. Peng, Y. Zhao, P. Jannasch and J. Yang, *J. Colloid Interface Sci.*, 2025, **686**, 304–317.
111 Z. Peng, T. Wei, Q. Wang, Y. Zhao and J. Yang, *J. Power Sources*, 2025, **642**, 236918.
112 A. N. Lai, S. C. Li, P. Z. Zheng, S. F. Zhou and S. J. Wu, *J. Appl. Polym. Sci.*, 2024, **141**, e55047.
113 J. Huang, Z. Yu, J. Tang, P. Wang, X. Zhang, J. Wang and X. Lei, *Colloids Surf., A*, 2023, **674**, 131890.
114 N. Li, T. Yan, Z. Li, T. Thurn-Albrecht and W. H. Binder, *Energy Environ. Sci.*, 2012, **5**, 7888–7892.
115 K. Zhang, S. Gong, B. Zhao, Y. Liu, N. A. Qaisrani, L. Li, F. Zhang and G. He, *J. Membr. Sci.*, 2018, **550**, 59–71.
116 J. Chen, C. Shen and S. Gao, *Desalination*, 2023, **557**, 116600.
117 J. J. Wang, W. T. Gao, Y. S. L. Choo, Z. H. Cai, Q. G. Zhang, A. M. Zhu and Q. L. Liu, *J. Colloid Interface Sci.*, 2023, **629**, 377–387.
118 X. Wu, N. Chen, H.-A. Klok, Y. M. Lee and X. Hu, *Angew. Chem.*, 2022, **134**, e202114892.
119 S. Lee, H. Lee, T.-H. Yang, B. Bae, N. A. T. Tran, Y. Cho, N. Jung and D. Shin, *Membranes*, 2020, **10**, 306.
120 S. Hosimin, V. Varshini, A. Kalaiyarasi, S. Vengatesan, S. Ravichandran, C. Djadocks and S. Vasudevan, *New J. Chem.*, 2023, **47**, 15987–15997.
121 J. H. Chen, X. B. Yue, Y. S. L. Choo, Z. Yu, X. H. Wang, X. L. Gao, W. T. Gao, Q. G. Zhang, A. M. Zhu and Q. L. Liu, *J. Power Sources*, 2023, **570**, 233014.
122 M. Mandal, G. Huang, N. U. Hassan, W. E. Mustain and P. A. Kohl, *J. Mater. Chem. A*, 2020, **8**, 17568–17578.
123 T. Caielli, A. R. Ferrari, S. Bonizzoni, E. Sediva, A. Capr, M. Santoro, I. Gatto, V. Baglio and P. Mustarelli, *J. Power Sources*, 2023, **557**, 232532.
124 T. Wang, Y. Zhao, R. Ma, L. Li, Q. Ling, X. Li, Y. Ding and H. Wei, *Synth. Met.*, 2023, **296**, 117385.
125 X. Wu, N. Chen, C. Hu, H.-A. Klok, Y. M. Lee and X. Hu, *Adv. Mater.*, 2023, **35**, 2210432.
126 N. Zhang, X. Li, P. Li and S. Tang, *Int. J. Hydrogen Energy*, 2023, 25972–25983.
127 M. Ju, Q. Ren, J. Xu, X. Chen, L. Meng, J. Lei, P. Zhao and Z. Wang, *Chem. Eng. J.*, 2023, **466**, 143023.
128 I. Arunkumar, R. Gokulapriyan, V. Sakthivel, A. R. Kim, M. S. Oh, J. Y. Lee, S. Kim, S. Lee and D. J. Yoo, *ACS Appl. Energy Mater.*, 2023, **6**, 7702–7713.
129 S.-B. Lee, C.-M. Min, J. Jang and J.-S. Lee, *Polymer*, 2020, **192**, 122331.
130 C. Hu, J. H. Park, H. M. Kim, H. H. Wang, J. Y. Bae, N. Y. Kang, N. Chen and Y. M. Lee, *J. Membr. Sci.*, 2022, **647**, 120341.
131 H. M. Kim, C. Hu, H. H. Wang, J. H. Park, N. Chen and Y. M. Lee, *J. Membr. Sci.*, 2022, **644**, 120109.
132 C. X. Lin, X. L. Huang, D. Guo, Q. G. Zhang, A. M. Zhu, M. L. Ye and Q. L. Liu, *J. Mater. Chem. A*, 2016, **4**, 13938–13948.
133 S. S. Patil, V. M. adhura, I. Kammakakam, M. H. Swamy, K. S. Patil, Z. Lai and A. R. HN, *Electrochim. Acta*, 2022, **426**, 140826.
134 L. Zhu, X. Yu and M. A. Hickner, *J. Power Sources*, 2018, **375**, 433–441.

135 B. Lin, F. Xu, Y. Su, J. Han, Z. Zhu, F. Chu, Y. Ren, L. Zhu and J. Ding, *ACS Appl. Energy Mater.*, 2019, **3**, 1089–1098.
136 M. S. Cha, J. E. Park, S. Kim, S.-H. Han, S.-H. Shin, S. H. Yang, T.-H. Kim, D. M. Yu, S. So and Y. T. Hong, *et al.*, *Energy Environ. Sci.*, 2020, **13**, 3633–3645.
137 T. H. Pham, J. S. Olsson and P. Jannasch, *J. Mater. Chem. A*, 2019, **7**, 15895–15906.
138 H. J. Park, S. Y. Lee, T. K. Lee, H.-J. Kim and Y. M. Lee, *J. Membr. Sci.*, 2020, **611**, 118355.
139 L. Wang, J. J. Brink, Y. Liu, A. M. Herring, J. Ponce-González, D. K. Whelligan and J. R. Varcoe, *Energy Environ. Sci.*, 2017, **10**, 2154–2167.
140 J. Zhang, K. Zhang, X. Liang, W. Yu, X. Ge, M. A. Shehzad, Z. Ge, Z. Yang, L. Wu and T. Xu, *J. Mater. Chem. A*, 2021, **9**, 327–337.
141 N. Chen, S. Y. Paek, J. Y. Lee, J. H. Park, S. Y. Lee and Y. M. Lee, *Energy Environ. Sci.*, 2021, **14**, 6338–6348.
142 W. Yuan, L. Zeng, S. Jiang, C. Yuan, Q. He, J. Wang, Q. Liao and Z. Wei, *J. Membr. Sci.*, 2022, **657**, 120676.
143 L. Liu, L. Bai, Z. Liu, S. Miao, J. Pan, L. Shen, Y. Shi and N. Li, *J. Membr. Sci.*, 2023, **665**, 121135.
144 W. T. Gao, X. L. Gao, W. W. Gou, J. J. Wang, Z. H. Cai, Q. G. Zhang, A. M. Zhu and Q. L. Liu, *J. Membr. Sci.*, 2022, **655**, 120578.
145 X. Hu, Y. Huang, L. Liu, Q. Ju, X. Zhou, X. Qiao, Z. Zheng and N. Li, *J. Membr. Sci.*, 2021, **621**, 118964.
146 I. Jeong, K. Min, H. Kim, S. Y. Nam and T.-H. Kim, *J. Membr. Sci.*, 2023, 122079.
147 M. Karibayev, S. Kalybekkyzy, Y. Wang and A. Mentbayeva, *Molecules*, 2022, **27**, 3574.
148 C. N. M. Ouma, K. O. Obodo and D. Bessarabov, *Membranes*, 2022, **12**, 1051.
149 F. Gu, H. Dong, Y. Li, Z. Si and F. Yan, *Macromolecules*, 2014, **47**, 208–216.
150 C. H. Park, T.-H. Kim, D. J. Kim and S. Y. Nam, *Int. J. Hydrogen Energy*, 2017, **42**, 20895–20903.
151 H. Takaba, T. Hisabe, T. Shimizu and M. K. Alam, *J. Membr. Sci.*, 2017, **522**, 237–244.
152 K. Zhang, W. Yu, X. Ge, L. Wu and T. Xu, *J. Membr. Sci.*, 2022, **661**, 120922.
153 F. Sepehr, H. Liu, X. Luo, C. Bae, M. E. Tuckerman, M. A. Hickner and S. J. Paddison, *Macromolecules*, 2017, **50**, 4397–4405.
154 I. Zadok, D. R. Dekel and S. Srebnik, *J. Phys. Chem. C*, 2019, **123**, 27355–27362.
155 T. Zelovich, L. Vogt-Maranto, C. Simari, I. Nicotera, M. A. Hickner, S. J. Paddison, C. Bae, D. R. Dekel and M. E. Tuckerman, *Chem. Mater.*, 2022, **34**, 2133–2145.
156 J. Pan, H. Zhu, H. Cao, B. Wang, J. Zhao, Z. Sun and F. Yan, *J. Membr. Sci.*, 2021, **620**, 118794.
157 M.-T. Lee, *J. Phys. Chem. C*, 2019, **123**, 10802–10815.
158 X. Luo and S. J. Paddison, *Solid State Ionics*, 2019, **339**, 115012.
159 R. Li, X. Chen, X. Zhou, Y. Shen and Y. Fu, *Sep. Purif. Technol.*, 2023, **314**, 123577.
160 D. J. Kim, C. H. Park and S. Y. Nam, *Int. J. Hydrogen Energy*, 2016, **41**, 7641–7648.
161 J. L. Di Salvo, G. De Luca, A. Cipollina and G. Micale, *J. Membr. Sci.*, 2020, **599**, 117837.
162 T. Zelovich, D. R. Dekel and M. E. Tuckerman, *J. Membr. Sci.*, 2023, **678**, 121638.
163 P. Sharma and A. P. Sunda, *ACS Appl. Polym. Mater.*, 2025, **7**, 1886–1895.
164 S. Chen, H. Wang, J. Zhang, S. Lu and Y. Xiang, *J. Membr. Sci.*, 2020, **605**, 118105.
165 W. Ma, Q. Liu, J. Li, L. Tian and H. Zhu, *Int. J. Hydrogen Energy*, 2023, **48**, 15258–15268.
166 C. Chen, C. Arntsen and Y.-L. S. Tse, *J. Chem. Phys.*, 2020, **152**, 094903.
167 K. Yassin, I. G. Rasin, S. Willdorf-Cohen, C. E. Diesendruck, S. Brandon and D. R. Dekel, *J. Power Sources Adv.*, 2021, **11**, 100066.
168 K. Yassin, J. C. Douglin, I. G. Rasin, P. G. Santori, B. Eriksson, N. Bibent, F. Jaouen, S. Brandon and D. R. Dekel, *Energy Convers. Manage.*, 2022, **270**, 116203.
169 R. Sharma, T. Chakraborti and J. K. Singh, *J. Memb. Sci.*, 2025, **736**, 124598.
170 W. Pu and Z. Sun, *Phys. Chem. Chem. Phys.*, 2025, **27**, 4634–4642.
171 Y. Yang, H. Huang, Z. Li, C. Xiao, M. U. Haq and L. Zeng, *Future Batteries*, 2025, **5**, 100016.
172 A. Sahul Hameed, S. Munusamy, R. Gokulapriyan and D. J. Yoo, *ACS Appl. Polym. Mater.*, 2024, **6**, 12341–12361.
173 N. Chen, C. Hu and Y. M. Lee, *Acc. Chem. Res.*, 2025, **58**, 688–702.
174 J. Xue, J. C. Douglin, K. Yassin, T. Huang, H. Jiang, J. Zhang, Y. Yin, D. R. Dekel and M. D. Guiver, *Joule*, 2024, **8**, 1457–1477.
175 J. Xue, J. C. Douglin, T. Huang, H. Jiang, J. Zhang, Y. Yin, D. R. Dekel and M. D. Guiver, *J. Membr. Sci.*, 2025, **717**, 123519.
176 W. K. Ng, W. Y. Wong, N. A. Rosli and K. S. Loh, *Separations*, 2023, **10**, 424.
177 C. Santoro, A. Lavacchi, P. Mustarelli, V. Di Noto, L. Elbaz, D. R. Dekel and F. Jaouen, *ChemSusChem*, 2022, **15**, e202200027.
178 G. A. Lindquist, S. Z. Oener, R. Krivina, A. R. Motz, A. Keane, C. Capuano, K. E. Ayers and S. W. Boettcher, *ACS Appl. Mater. Interfaces*, 2021, **13**, 51917–51924.
179 J. Lim, J. M. Klein, S. G. Lee, E. J. Park, S. Y. Kang, S. Maurya, W. E. Mustain, S. Boettcher and Y. S. Kim, *ACS Energy Lett.*, 2024, **9**, 3074–3083.
180 S. Dagar and A. P. Sunda, *Mol. Syst. Des. Eng.*, 2026, **11**, 255–268.
181 K. Yassin, I. G. Rasin, S. Brandon and D. R. Dekel, *J. Membr. Sci.*, 2024, **690**, 122164.